

Application of in vivo methodologies to investigation of biological structure, function and xenobiotic response in see-through medaka (*Oryzias latipes*)

Ron C. Hardman*, Seth.W. Kullman and David E. Hinton

Duke University, Nicholas School of the Environment and Earth Sciences, Division of Environmental Science and Policy, Durham NC, USA

Key words: medaka, liver, toxicity, hepatobiliary, in vivo imaging

Abstract We describe here the development and application of non invasive in vivo methodologies to the investigation of biological structure, function and xenobiotic response in see-through medaka (STII; *Oryzias latipes*). In vivo studies in STII medaka provided novel insights into hepatobiliary architecture, development and toxic response, in both 2 and 3 dimensions. As the presented findings suggest, STII medaka provide a unique means for high resolution in vivo study, and the future opportunity to integrate mechanisms of toxicity (e.g. genomic, proteomic information) with phenotypic changes at the system level (the overarching goal of our laboratory). While our focus has been the hepatobiliary system, other organ systems are equally amenable to in vivo study, and we consider the potential for discovery, within the context of in vivo investigation in STII medaka, as significant.

Introduction

Exhibiting no expression of leucophores and melanophores, and minimal expression of xanthophores and iridophores, see-through medaka (STII) are essentially transparent throughout their life cycle (Wakamatsu *et al.* 2001), and allow high resolution (< 1µm) non invasive in vivo imaging of internal organs and tissues at the subcellular level. By comparison, other medaka stocks develop dermal and visceral pigmentation that precludes high resolution widefield and confocal imaging deep within organisms. Employing widefield and confocal microscopy technologies, in conjunction with fluorescent probes, we developed methodologies for high resolution in vivo imaging at the subcellular level. In embryo, larval and juvenile STII medaka (from 3 to 60 days post fertilization, dpf)

it is possible to view cells and tissues internally (resolving features < 1 µm in size), and to generate 3D reconstructions of organs and tissues under study.

Because our focus was the hepatobiliary system, we use as an example, and provide a summary of, our studies in this organ system in vivo, from organogenesis through embryonic and larval stages of development.

Materials and Methods

Medaka

See-through medaka (STII) were provided by Prof. Y. Wakamatsu, Laboratory of Fresh Water Fish Stocks, Nagoya University. Our STII medaka colony, maintained at Duke University since 2002, are housed in a charcoal filtrated, UV treated re-circulating system (City of Durham, NC water) maintained at 25 +/- 0.5°C. Water chemistries were maintained at: pH (7.0–7.4), dissolved oxygen (6–7 ppm), ammonia (0–0.5 ppm), nitrite (0–0.5 ppm) and nitrate (0–10 ppm). Water hardness was maintained at 80–100 mg L⁻¹ CaCO₃, following guidelines of the US EPA (Horning and Weber 1985). A diel cycle of 16:8 hr (light:dark) was employed. Medaka larvae were fed ground (pressed through a 60 µm sieve) Otohime β diet (Ashby Aquatics, West Chester, PA) via an automatic feeder 7 times per day. Because Otohime β has been shown to be free of estrogenic complications (Inudo *et al.* 2004), we considered it an optimal fish food. In addition, all brood stock fish diets were supplemented daily with Artemia nauplia (hatched brine shrimp). Egg clusters, collected daily, were cleaned in embryo rearing medium (ERM), and individual fertilized eggs were separated and maintained in ERM at 25°C.

* Correspondence to: Dr. Ron C. Hardman, Duke University, Nicholas School of the Environment and Earth Sciences, Box 90328, LSRC A333B, Duke University, Durham, NC 27708-0328, USA, Tel.: 1-919-613-8038, Fax: 1-919-684-8741, Email: ron.hardman@duke.edu

Unconsumed diet, detritus and associated algal material were removed from rearing and brood stock tanks daily. Care and maintenance of medaka were in accordance with protocols approved by the Institutional Animal Care and Use Committee (IACUC; A117-07-04; A141-06-04; A173-03-05).

Microscopy

A Zeiss Axioskopp equipped with DAPI/TRITC/FITC fluorescence filter cube set (DAPI/UV: Ex 360–380nm / Em All Vis >400nm, FITC: Ex 450–490nm / Em 515–565nm, TRITC: Ex 528–552nm / Em 578–632nm), Zeiss Plan Neofluars 5x/0.15, 10x/0.3, 20x/0.5, 40x/0.85 pol, and 100x/1.3 oil objectives, Photometrics CoolSnap digital imaging system (2048 x 2048-element array) and IP Lab (V. 3.0) image acquisition software (Scanalytics) was used for widefield fluorescence microscopy. A xenon lamp was used for excitation. (DAPI-4'-6-Diamidino-2-phenylindole, TRITC-tetramethylrhodamine isothiocyanate, FITC-fluorescein Isothiocyanate).

For confocal fluorescence microscopy a Zeiss 510 Meta system with Zeiss LSM 5 Axiovision image acquisition software, Argon and HeNe laser and Carl Zeiss C-apochromatic 40x/1.2, C-apochromatic 10x/0.45 objectives was used.

A Nikon Eclipse E600 with a Nikon DXM 1200 digital capture system, halogen light source, Nikon plan neo-fluor 10x/0.3 wd16, plan neo-fluor 20x/0.5 wd2.1, plan neo-fluor 40x/0.75 wd0.72, and plan apo 60x/1.4 wd0.21 (oil) objectives was used for brightfield microscopy. A Nikon SZM 1500 (dissecting microscope) with a Nikon DXM 1200 digital capture system, Nikon HR plan apo 1x WD54 and Nikon HR 0.5x WD136 objectives was used for brightfield microscopy.

Software: Image analysis and compilation were performed with EclipseNet (Nikon, USA), Adobe Photoshop (Adobe, Inc.), ImageJ (V1.32j), IP Lab software (Scanalytics, Inc., version 3.55), and Zeiss Image Browser (Carl Zeiss). All 3 dimensional reconstructions and analyses were performed with Amira 3D (Mercury Computer Systems, Berlin).

All transmission electron microscopy (TEM) was performed at the Laboratory for Advanced Electron and Light Optical Methods (LAELOM), College of Veterinary Medicine, North Carolina State University, on an FEI/Philips EM 208S Transmission Electron Microscope.

Chemicals and fluorescent probes

A full list of fluorescent probes used is shown in Table 1. The primary fluorescent probes employed were; 7-benzyloxyresorufin, β -Bodipy C5-HPC [BODIPY® 581/591 C5-HPC (2-(4,4-difluoro-5-(4-phenyl-1,3-butadienyl)-4-bora-3a,4a-diaza-s-indacene-3-pentanoyl)-1-hexadecanoyl-sn-glycero-3-phosphocholine)], Bodipy FL C5-ceramide [N-(4,4-difluoro-5,7-dimethyl-4-bora-3a,4a-diaza-s-indacene-3-pentanoyl) sphingosine], DAPI [4',6-diamidino-2-phenylindole, dihydrochloride], and fluorescein isothiocyanate. All fluorescent probes were administered to STII medaka via aqueous bath in concentration ranges listed in Table 1. Duration of exposure times (aqueous bath exposures) varied for each fluorescent probe, and can be derived from the values given in initial and peak exposure column.

Embryo rearing medium (ERM) was prepared as follows: 1.0 ml Hank's Stock #1, 0.1 ml Hank's Stock #2, 1.0 ml Hank's Stock #4, 1.0 ml Hank's Stock #5, 1.0 ml fresh Hank's Stock #6, in 95.9 ml distilled H₂O, pH 7.2 [Stock #1: 8.0 g NaCl, 0.4 g KCl, in 100 ml distilled H₂O, Stock #2: 0.358 mg Na₂HPO₄ Anhydrous, 0.60 mg KH₂PO₄, in 100 ml ddH₂O, Stock #4: 0.72 g CaCl₂ in 50 ml ddH₂O, Stock #5: 1.23 g MgSO₄·7H₂O in 50 ml distilled H₂O, Stock #6: 0.35 g NaHCO₃ 10.0 mls distilled H₂O]. Other chemicals employed: Diethylnitrosamine (N-nitrosodiethylamine, Sigma, N0756), ethinyl estradiol [(1,3,5 (10)-estratriene-3, 17 β -diol), Sigma, E-8875], α -naphthylisothiocyanate (Sigma, N4525), β -naphthoflavone (Sigma, N-3633), tricaine-methane sulfonate (Sigma, E10521), dimethylsulfoxide (DMSO) (Sigma, 276855), Pronase (streptococcal protease, Sigma), Hank's balanced salt solution (Sigma, H5899), phosphate buffered saline (PBS, sigma).

Statistics

Differences in fluorescence intensity in digital image captures were analyzed statistically using Statview software (SAS institute, Cary, NC). Two way ANOVA with Fisher's T-test was employed to assess statistically significant differences in fluorescence intensity. Background fluorescence and autofluorescence was accounted for in statistical analyses. Pearson's Correlation Coefficient was used for comparison of calculated versus measured morphometric values in vivo. Equality of Variance F-test was used for assessment of blood to bile transport, which was assessed via comparison of

Table 1. Fluorescent Probes

Fluorophore	Soluble	Ex	Em	Initial/ Peak Assimila- tion Time (min)	Exposure Concent- ration
7-benzyloxyresorufin In vivo CYP3A activity. Uptake via gill, in vivo metabolism in gill and gut, good for investigating blood to bile transport, IHBPs, EHBP and intestinal lumen.	DMSO	560	590	30/45	50 μ M
7-Ethoxyresorufin In vivo imaging of CYP1A activity. Uptake via gill, in vivo metabolism in gill and liver. CYP 1A2, 2E Substrate.	DMSO			30/45	10–50 μ M
Acridine Orange In vivo labeling of DNA, RNA. Good for apoptosis, interacts with DNA and RNA by intercalation or electrostatic attractions.	H ₂ O	500	526		1–5 μ M
BODIPY 505/515: 4,4-difluoro-1,3,5,7-tetramethyl-4-bora-3a, 4a-diaza-s-indacene Uptake via gill, active transport through hepatobiliary system, concentrative blood to bile transport, and secretion from gall bladder into gut lumen. Good for elucidation of gill, IHBP, EHBP, intestinal lumen. Non-Polar, Lipophilic.	DMSO	502	510	15/20	5 μ M–100 nM
BODIPY FL C5-ceramide: N-(4,4-difluoro-5,7-dimethyl-4-bora-3a, 4a-diaza-s-indacene-3-pentanoyl)sphingosine Putative passive transport in vivo. Uptake via gill, transport through cardiovascular and hepatobiliary systems and secretion from gall bladder into gut lumen.	DMSO	358	461	20/45	5 μ M–100 nM
Bodipy Verapamil In vivo Bodipy verapamil localized to hepatocytic cytosol in discrete vesicles. Transport to bile was not observed in the time frame assayed, which was 90 minutes.	DMSO	504	511	20/60	
BODIPY® 493/503: 4,4-difluoro-1,3,5,7,8-pentamethyl-4-bora-3a, 4a-diaza-s-indacene (BODIPY® 493/503) Uptake via gill, active transport through hepatobiliary system, concentrative blood to bile transport, and secretion from gall bladder into gut lumen. Good for elucidation of gill, IHBPs, EHBP, intestinal lumen. Lipophilic, amphiphilic.	DMSO	493	504	15/20	10 μ M
BODIPY® 581/591 C5-HPC (Phosphocholine) PC: 2-(4,4-difluoro-5, 7-dimethyl-4-bora-3a,4a-diaza-s-indacene-3-pentanoyl)-1-hexadecanoylsn-glycero-3-phosphocholine In vivo labeling of intrahepatic and extrahepatic biliary system. Uptake via gill. Hepatobiliary transport to gut lumen. Diffuse fluorescence in hepatocyte cytosol.	DMSO	582	593	15/20	30 nM
CellTrace™ Oregon Green® 488 carboxylic acid diacetate, succinimide ester (carboxy-DFFDA, SE) *cell permeant* *mixed isomers In vivo labeling of hepatic nuclei, potential for detection of apoptosis.	DMSO	<300	none	15/20	10–100 μ M
DAPI: 4',6-diamidino-2-phenylindole, dihydrochloride In vivo nuclear labeling of virtually all cell types associated with gill, gut, liver, and cardiovascular system.	H ₂ O, DMF	358	461	15/60	0.3–3.0 μ M
DAPI Diacetate: 4',6-diamidino-2-phenylindole, diacetate DAPI diacetate is water-soluble form. In vivo nuclear labeling.	H ₂ O, MeOH	358	461	15/60	0.3–3.0 μ M
Fluorescein-5-isothiocyanate (FITC 'Isomer I') Excellent in vivo probe for elucidating biliary system. In vivo labeling of intrahepatic and extrahepatic biliary system. Hepatobiliary transport to intestinal lumen. Uptake via gill.	DMSO	494	519	10/30	1 μ M - 50 nM
MitoTracker® Green FM In vivo labeling of hepatocytes.	DMSO	490	516	20/30	25–200 nM
SYTO® 16 green fluorescent nucleic acid stain In vivo nuclear labeling of epithelia and endothelia, putative in vivo probe for apoptosis.	DMSO	488	518	15/30	10 nM–1 μ M
SYTO® 27 green fluorescent nucleic acid stain Apoptosis.	DMSO	495	537	15/50	10 nM–1 μ M
SYTOX® Orange nucleic acid stain Apoptosis	DMSO	547	570	15/50	0.1–5 μ M
YO-PRO®-1 iodide (491/509) Apoptosis	DMSO		509	15/60	1 μ M
YOYO-1 Iodide (491/509) In vivo accumulated in interstitial spaces, some labeling of vasculature. Typically used for assays for cell enumeration, cell proliferation and cell cycle.	DMSO	491	509	15/50	2–5 nM

28 fluorescent probes were selected for in vivo application based on their molecular weight, utility in elucidating desired structure/function, on their biocompatibility, and in vivo transport properties (18 probes are shown). The fluorescent probe, a description of findings, solvent used for stock preparation (solubility), fluorescence excitation and emission wavelengths (Ex/Em), initial and peak fluorescence times, and effective aqueous exposure concentrations are given.

fluorescence intensities across sinusoid, hepatocytic cytosol and canalicular spaces. Descriptive statistics were used for morphometric analyses.

Histology and immunohistochemistry

All histological sections were prepared by the Histopathology Laboratory, College of Veterinary Medicine, North Carolina State University. For histological studies medaka were fixed in 10% formalin for 24 hrs. Medaka younger than 20 dpf were fixed whole. For medaka older than 20 dpf, a midline incision was made from the anal aperture to the level of the head kidney, to allow saturation of abdominal cavity with fixative. Cytokeratins 7, 8, 18 and 19 (Invitrogen) and alpha fetoprotein (AFP) primary antibodies were used for investigation of hepatocyte, biliary epithelia and bile ductular epithelia (cytokeratin profile, cell differentiation). Secondary antibodies were; Alexa-Fluor 488 goat anti-mouse IgG and Alexa-Fluor 488 IgG (Fab fragment). Cryo sections and paraffin imbedded sections were incubated with primary antibodies at dilutions of 1:100 to 1:200 (PBS) for 90 minutes at room temperature. Sections were washed three times with PBS after incubation with primary antibodies, incubated with secondary antibodies for 90 minutes at room temp, and subsequently washed three times with PBS. Sections were mounted in Ultracruz mounting medium and examined using a Zeiss Axioskopp fluorescence microscope.

Xenobiotic exposures

ANIT and DEN exposures were in aqueous bath at various stages of development, under acute, chronic and serial exposure conditions. Acute exposures: medaka were exposed once to aqueous concentrations of 0.25 μ M to 10 μ M ANIT, and assessed at 6, 12, 24, 48, 72 and 96 hrs, and at day 10, 30 and 60 post exposure. Serial/chronic exposures: time points for exposures are the same as described for acute exposure conditions, however, for serial exposures, medaka were re-dosed every 3 days, or once weekly, and examined at the same points given for acute exposure. For serial exposures static renewal was used with replacement of solution every three days. Controls received DMSO (ANIT, DEN solvent) at same exposure concentrations given for ANIT, DEN. DEN exposure was for 48 hrs at 200 ppm in aqueous bath. All exposures were done in 750 ml wide-bottom glass rearing beakers. Aqueous bath/exposure medium was ERM:deionized water

(1:3). Glass rearing beakers were kept on a 28° C heating pad. Cohorts of medaka ranged from 10 to 30 fish, depending on the study. From each cohort of medaka subpopulations were used for; *in vivo* assessments, histological and immunohistochemical studies, and transmission electron microscopy (TEM) studies.

Results and Discussion

As an overview: *in vivo* study (methodology) in STII medaka can be considered to be comprised of three primary components; (1) sedation, (2) microscopy/imaging technologies, and (3) fluorescent probes. First, we describe each in the context of methodology development, and then we give examples of the application of these tools to investigating biological structure/function and adaptive/toxic responses of the hepatobiliary system, *in vivo*.

Sedation

For optimal *in vivo* imaging of larval and older STII medaka (> 8dpf) we found non lethal sedation necessary, particularly when working/imaging at the cellular level. While an ice bath proved effective for sedation of medaka at all stages of development, optimal sedation was achieved with 10 μ M tricaine methane-sulfonate (MS-222). Briefly; STII medaka were placed in a solution of 10 μ M MS-222 (ERM as solvent). As soon as medaka were anaesthetized (immobile) they were removed from the sedative bath to a bath of fresh ERM:deionized water (1:3) for 1 – 2 minutes. Sedated medaka were then placed on a glass depression well slide with ~ 400 μ l of ERM:deionized water, or enough solution to fill the depression well, oriented in a desired anatomical position, and cover-slipped with #2 glass cover-slips. Sedated medaka were completely immersed in an aqueous medium while cover-slipped on the depression well glass slide. Careful attention was paid to ensuring medaka were as close to the cover-slip as possible. This entailed positioning sedated medaka as close to the edge of the concave depression well as possible, thereby ensuring contact of the dermis with the cover-slip. Such positioning minimized the fluid medium between medaka and cover-slip. Even small distances of a few microns between medaka and the cover-slip greatly diminished optical resolution (clarity of cells and tissues), due to diffraction of the image through the intervening space.

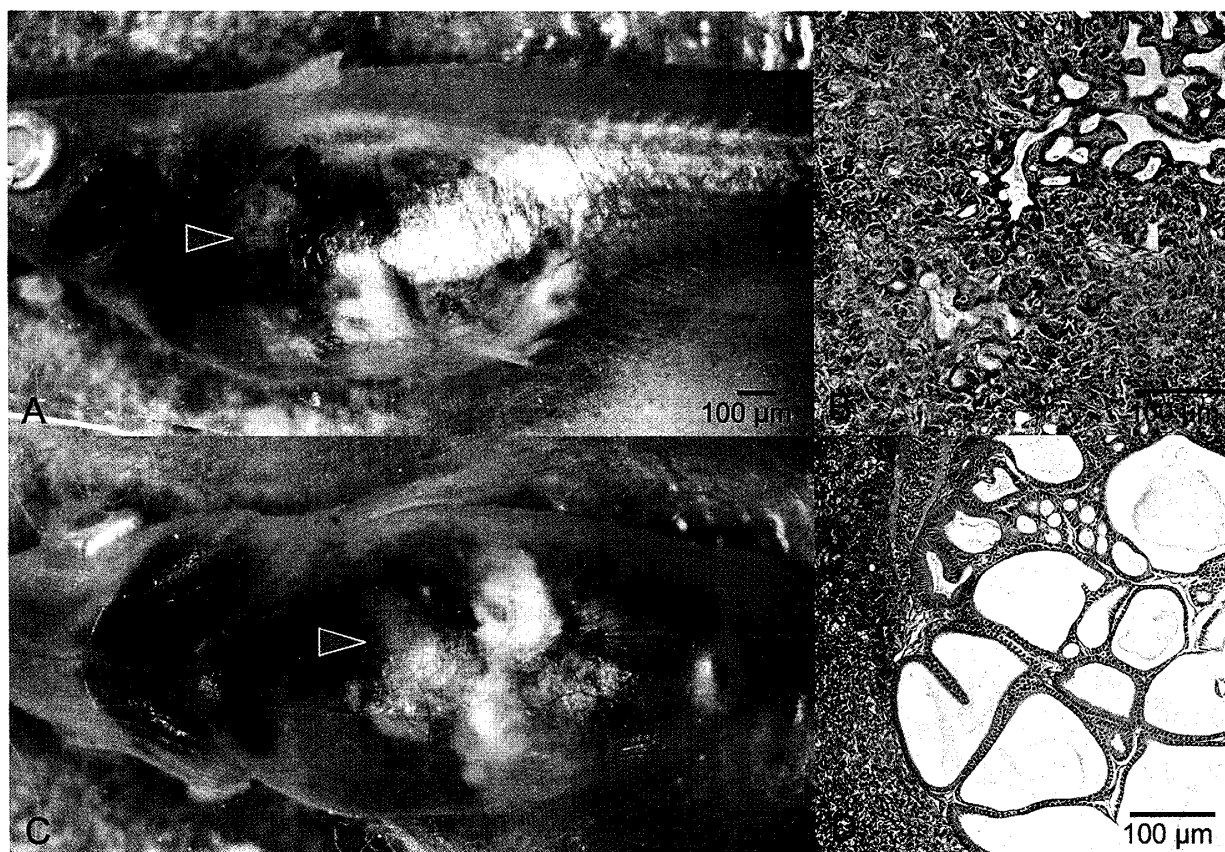


Figure 1. In vivo imaging of tumor formation in STII medaka: brightfield microscopy. Neoplastic response following early life stage exposure of STII medaka to the reference hepatocarcinogen diethylnitrosamine (DEN). (A & C) In vivo imaging (bright-field) of hepatic tumor formation (green arrowheads) in medaka exposed to DEN at an early life stage, showing enlargement of total liver mass and altered vasculature. Histopathological assessment of the tumor showed mixed hepatocellular (B) and cholangiocellular carcinomas (D). Biliary hyperplasia (D) was characterized by a single layer of biliary epithelium lining large cystic spaces in the liver. Opaque white tissue in brightfield images (A&B) is ovary, the gut occupies caudal most region of the abdominal cavity.

Microscopy/imaging techniques

Once mounted on a depression well glass slide medaka were imaged live with brightfield, wide-field and laser scanning confocal fluorescence microscopy (LSCM). Each presented specific advantages and disadvantages, which will be illustrated through the in vivo images presented here. Following, we present an overview of considerations for each imaging modality.

Brightfield microscopy (e.g. Nikon LSM dissecting microscope), due to optics and illumination source, was well suited for investigation at the tissue and organ level of organization. An example is shown in Figure 1; where hepatic tumor formation, the result of early life stage exposure to the carcinogen DEN, was imaged at 10 months post exposure through the abdominal wall. The ability to observe/image gross anatomy/whole animal via brightfield microscopy also provided a valuable comparative reference for fluorescence based imaging studies (e.g. LSCM, examples

can be seen throughout the images presented). Expectedly, brightfield microscopy (dissecting microscope) was not suitable for deep tissue observations in STII medaka, or for cellular level investigation/imaging.

Both widefield and confocal fluorescence microscopy proved excellent for high resolution (< 1 μm) in vivo observation/imaging of individual cells, tissues and organs in living individuals. While confocal microscopy was superior to widefield in virtually all aspects, as will be shown in the findings presented here, widefield microscopy was not without merit and should be considered a practical means by which to undertake in vivo investigations in STII medaka. For instance, widefield microscopy was at times employed as a screening method, and for methodology refinement, when access to a confocal microscope was not possible (a problem not uncommon in many research facilities). The fundamental drawback to widefield was optical resolution; an undesired

greater depth of field, and resolution inferior to that obtained with confocal microscopes.

By example: *in vivo* investigations into hepatobiliary transport (discussed later) necessitate the spatial resolution provided by confocal imaging. Because of the lack of resolution (depth of field permitted with Xenon laser and standard Neo-Fluar objectives, see materials and methods), widefield fluorescence microscopy was limited to qualitative studies (vs. quantitative *in vivo* study/imaging). The depth of field with the 60X Plan Neo-Fluar objective on our Zeiss Axioskopp (widefield) was 0.65 μm ; technically, comparable to confocal. However, this 0.65 μm depth of field represents only the field of fine focus. Also resolved, due to illumination by Xenon laser lighting source, were out of focus planes above and below the plane of focus. It follows that due to reflection and refraction from tissues above and below the plane of imaging, optical resolution was diminished, and fluorescence based studies were limited to semi-quantitative and qualitative assessments.

In contrast, confocal microscopy (LSCM), due to limited depth of field and optical resolution, proved optimal for quantitative *in vivo* investigations into hepatobiliary transport (transport of fluorophores from blood to bile). Confocal microscopy also offered the advantage of acquisition of confocal stacks of up 100 μm in depth, at planes of section from 0.5 μm to 2 μm . Further, individual confocal stacks could be coupled, allowing for final *in vivo* confocal image stacks of up 200 μm in depth (the maximal depth, we found, at which high quality *in vivo* imaging could be performed) with the system used.

In summary, while widefield was sufficient for qualitative study/imaging of hepatobiliary structure, function and transport, accurate quantitative study/imaging required the finer spatial resolution provided by LSCM. Confocal microscopy permitted high resolution *in vivo* imaging of individual cells, and subcellular organelles, and enabled 3 dimensional reconstructions (3D) of the hepatobiliary system via acquisition of *in vivo* confocal imaging stacks (described in detail below). Examples illustrating the differences between widefield and confocal microscopy can be seen throughout the findings presented here.

Fluorescent probes and endogenous fluorophores

Importantly, fluorescence-based microscopy

proved highly valuable to *in vivo* investigations. The use of fluorescent probes in living medaka greatly enhanced our ability to investigate hepatobiliary structure/function and xenobiotic response *in vivo*. While fluorescent probes have been widely employed *in vitro* (e.g. cell culture based investigations), few commercially available fluorophores were (at the time the studies were undertaken) characterized for *in vivo* use in fish. Hence, a large part of our work was the exploration of fluorophores that could be employed for *in vivo* investigation in medaka (biocompatibility, efficacy). 43 fluorescent probes were screened, of these, 28 were found to be useful probes for elucidation of biological structure and function. Fluorophores selected for biocompatibility and utility in analysis of hepatobiliary morphology and transport are given in Table 1. Probes were also selected on their ability to be administered via aqueous bath, and to provide for evaluation of *in vivo* transport dynamics/kinetics. That a probe would exhibit uptake, transport and distribution via aqueous bath was a priority for selection. Other options for fluorophore administration were via intra-peritoneal or intravenous injection (IP, IV). Because many studies were carried out during developmental phases, this would entail IP, IV, or yolk sac injection in embryos and larvae, requiring microinjection techniques; a route of administration that would prove time consuming, would significantly extend the time required for *in vivo* investigations, and that in some instances may prove harmful to medaka under study (e.g. embryos, larvae). IP injections can also be inconsistent in delivery of the agent introduced (e.g. injections may occur within the gut lumen, or peritoneal cavity, thus altering uptake and transport kinetics of fluorophore, toxicant introduced). For these reasons aqueous bath exposures were employed as the route of administration for all fluorophores and toxicants described herein.

A descriptive overview of all probes is not possible in one report. Hence, for clarity, the properties of each probe are summarized in Table 1 and their efficacy can be derived from the findings presented in following sections. However, a discussion of selected fluorescent probes most frequently employed for elucidation of cell/tissue/organ structure and function is merited. Metabolic substrates 7-benzyloxyresorufin (7-BR, CYP3A substrate) and 7-ethoxyresorufin (7-ER, CYP1A substrate) were found to be valuable *in vivo* probes for investigating CYP3A and CYP1A

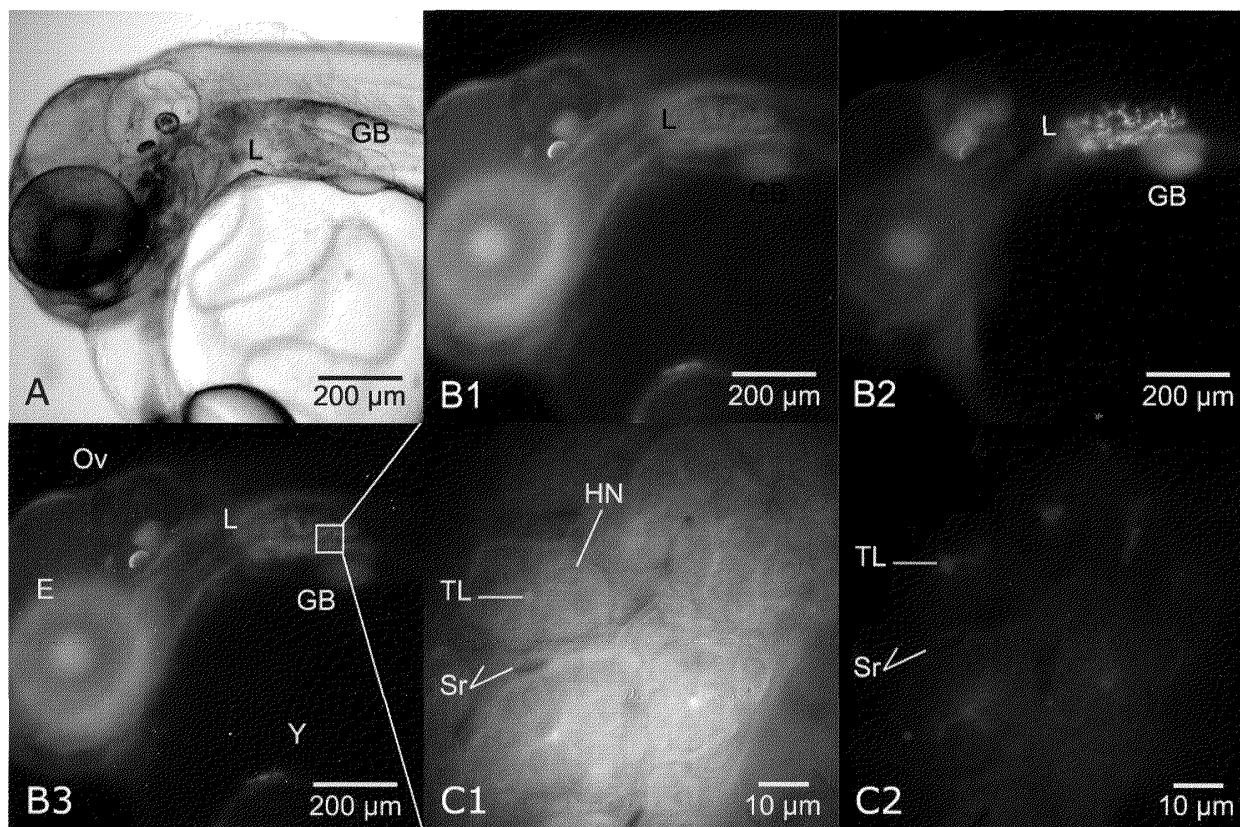


Figure 2. In vivo imaging of hepatobiliary metabolism, bile transport, and parenchymal architecture: widefield fluorescence microscopy. Illustrated is utilization of tissue autofluorescence and the in vivo application of 7-benzoyloxyresorufin (7BR) for detection of CYP3A metabolic activity. Dechorionated embryos exposed (aqueous bath) to the CYP3A substrate 7BR exhibited 7-benzoyloxyresorufin-O-dealkylation (BROD) activity, which resulted in the generation of the fluorescent metabolite resorufin (red). Transport of the metabolite through the intrahepatic biliary passageways (TL) of the embryonic liver (L), and concentration in the gall bladder (GB), was imaged in vivo in living dechorionated embryos. Hence, utilizing autofluorescence properties of tissues in tandem with fluorescent probes aided in vivo elucidation of biological structure and function. All in vivo images from an individual STII medaka, 6 dpf. (A) Brightfield microscopy, illustrating liver (L) and gall bladder (GB). (B1) Same animal as in frame A, imaged with widefield fluorescence microscopy (DAPI/UV) illustrating tissue autofluorescence. (B2) Same animal as frame A: Widefield fluorescence (TRITC) image capture of resorufin (indicative of CYP3A metabolic activity) fluorescence in the intrahepatic biliary passageways of the embryonic liver (L). Resorufin fluorescence is distinct and limited to the intrahepatic biliary passageways and gall bladder. (B3) Color composite of B1 & B2, DAPI/TRITC image captures, illustrating resorufin fluorescence (red) in the liver and gall bladder. (C1 & C2) In vivo imaging of hepatic parenchyma, 6dpf, revealing hepatic tubule phenotype. 6 to 8 hepatocytes were observed (in transverse section) to form a tubule lumen (TL) at their apical membranes. C2 shows concentrative transport of resorufin from hepatocellular cytosol to tubule lumen (TL), indicated by increased fluorescence in the tubule lumen. Red blood cells were observed actively circulating through hepatic sinusoids (S/r). Hepatocyte nuclei (HN).

expression in organs and tissues, and for elucidating the intra and extrahepatic biliary system, as well as gut lumen. Both probes, non-fluorescent in their native state, are metabolically activated (dealkylation of 7-BR, de-ethylation of 7-ER) by their respective CYP enzymes to the anionic fluorescent metabolite resorufin. Each have been widely employed in vitro in microsome and cell culture based assays (Miller *et al.*, 2000; Schlenk *et al.*, 1997; and others). 7-ER has also been employed for in vivo CYP1A activity in *Fundulus heteroclitus* and medaka (Willett *et al.* 1995; Meyer *et al.* 2002; Nacci *et al.* 2002; Kashiwada *et al.* 2007). Examples of in vivo applications of 7-BR, eluci-

dating in vivo metabolism, transport, and hepatic tubule phenotype are given in Figure 2.

Sphingolipids, a structurally diverse class of compounds composed of a polar head group and two nonpolar tails (akin to phospholipids), are naturally-occurring compounds found in all plants and animals. As such, there is potential for fluorescently-labeled sphingolipids to be incorporated into live cells. Two fluorescent sphingosines, β -Bodipy C5-HPC and Bodipy FL C5 Ceramide, were explored. β -Bodipy C5-HPC, a fluorescently-labeled phosphocholine, proved biocompatible and exhibited in vivo properties that were optimal for elucidating epithelia, endothelia, and hepato-

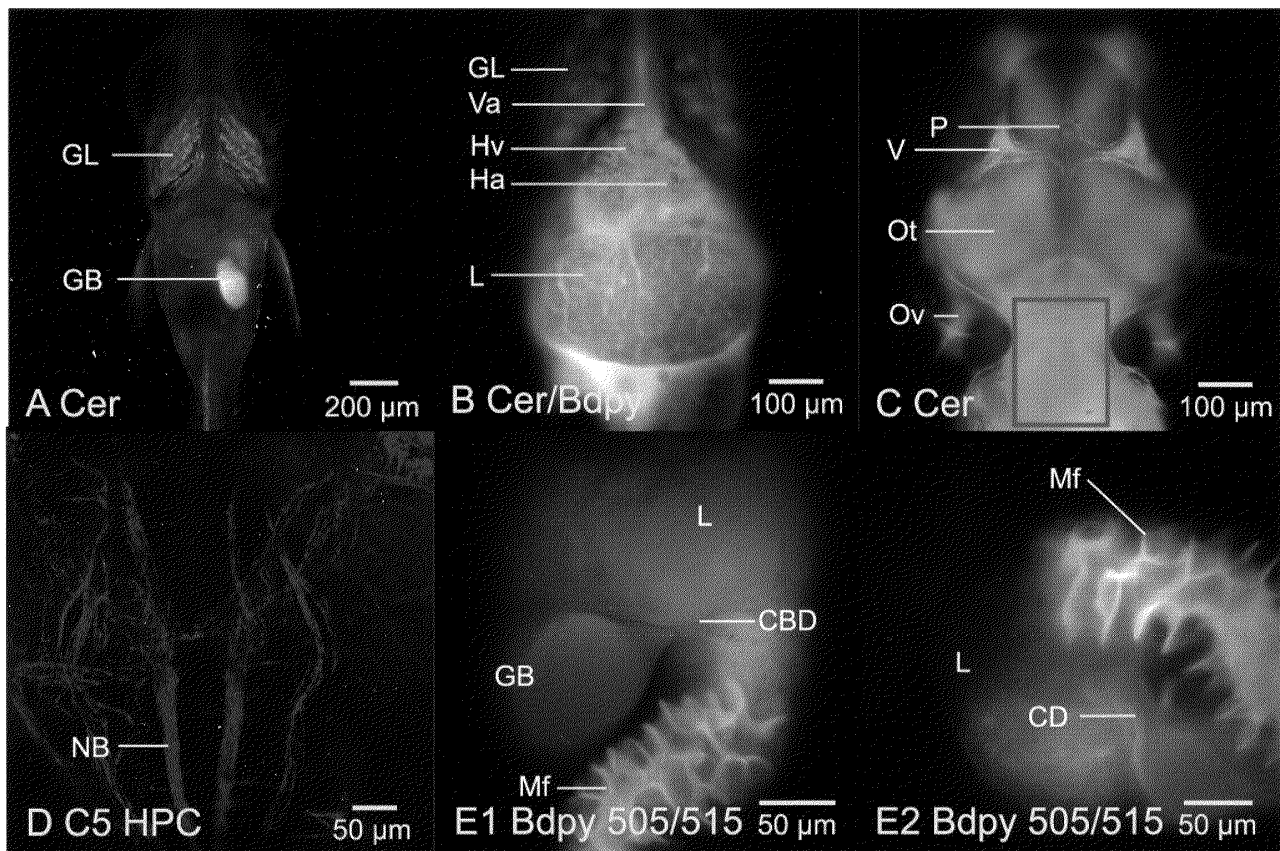


Figure 3. Differential uptake and transport of fluorescent probes β -Bodipy C5-HPC, Bodipy FL C5 and Bodipy 505/515: widefield and confocal fluorescence microscopy. (A - C) β -Bodipy C5 Ceramide uptake and distribution: (A & B) The ceramide fluorophore (green) exhibited properties consistent with passive diffusion across cell membranes, with distinct uptake over the gill (GL) and transport through the cardiovascular system. The fluorophore was not observed to cross the blood-brain barrier (C), though it persisted in vasculature, with a residence time of hours to days (depending on exposure regime). (D) In contrast, β -Bodipy C5 phosphocholine (HPC) was observed to label neurons in the hind brain of STII medaka. (D) STII medaka, 18dpf, confocal fluorescence microscopy (from 3D projection) of β -Bodipy C5 phosphocholine labeling neural bundles in the corpus cerebelli, crista cerebellaris and medulla, 90 minutes post fluorophore exposure (aqueous bath). Corpus cerebelli, crista cerebellaris and medulla are region of interest indicated by gray rectangle in frame C. (E1 & E2) Widefield fluorescence microscopy of Bodipy 505/515 secretion (red fluorescence) from gall bladder (GB) through the cystic duct (CD) and common bile duct (CBD) into the gut lumen. Mucosal folds of the gut (Mf) elucidated with β -Bodipy C5 Ceramide (green fluorescence; co-administered with Bodipy 505/515). Ventral aorta (Va), Heart Ventricle (Hv), Heart Atrium (Ha), Liver (L), Pineal Gland (P), Optic Tectum (Ot), Otic Vesicle (Ov), Vasculature (V).

biliary transport. β -Bodipy C5-HPC labeled the majority of all epithelia throughout the body of STII medaka. While *in vivo* dynamics/kinetics for fluorescently-labeled sphingosines like β -Bodipy C5-HPC and Bodipy FL C5 Ceramide are not currently known, and little information exists on their *in vivo* metabolic properties, *in vivo* observations suggest the fluorescently labeled β -Bodipy C5-HPC behaves as an endogenous sphingolipid, as β -Bodipy C5-HPC was readily incorporated into virtually all cell membranes under aqueous exposure conditions. For instance, β -Bodipy C5-HPC was not only taken up by virtually all epithelia, but observed to cross the blood brain barrier, labeling neural bundles in the medulla of medaka (Figure 3). β -Bodipy C5-HPC appeared to be taken up across gill epithelium, and trans-

ported through the cardiovascular system to the liver and gut. As a small organic cation the *in vivo* kinetics of this probe suggested concentrative transport of the fluorophore from blood to bile (hepatic), with fairly rapid (15 minutes post exposure) accumulation of the fluorophore in bile. While empirical and preliminary quantitative studies suggest concentrative vectorial transport of this fluorophore, further study will be necessary to elucidate the mechanisms of transport.

In contrast, the *in vivo* kinetics of Bodipy FL C5 ceramide appeared more consistent with passive diffusion across cell membranes. Uptake and distribution of the fluorophore was observed to be substantially slower (15–30 minutes slower) than β -Bodipy C5-HPC. Whereas the fluorescent phosphocholine (HPC) saw uptake and concentra-

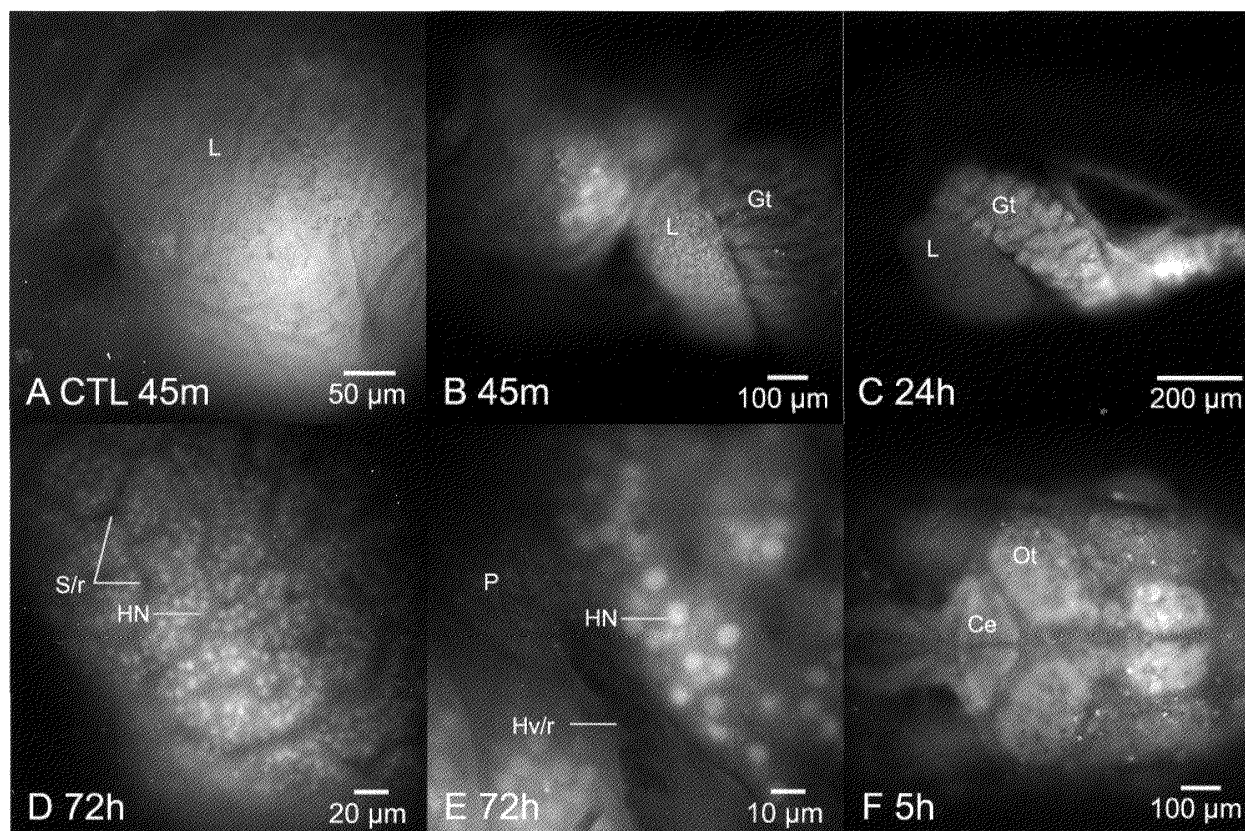


Figure 4. In vivo imaging of nuclear labeling. Evidence for in vivo metabolism and nuclear labeling of an experimental anti-malarial pro-drug, DB289, demonstrates non invasive in vivo imaging of nuclear binding of exogenous compounds. The anti-trypansosomal diamidine was used for preliminary investigation into the study of absorption, distribution, metabolism and excretion (ADME), as well as toxicity, in STII medaka. Preliminary results with two DB compounds (DB289 and DB75) suggest metabolism of the parent compound DB289 and nuclear binding of the active fluorescent metabolite (DB75) to olfactory tissues and hepatocytes within 15 minutes of aqueous exposure. ADME assessments showed temporal variation in nuclear binding, with distribution proceeding from liver (L), to gut (Gt) and pancreas (P), and eventually systemic tissues, over a 24 hr period. In rodent and primate models DB289 is metabolized (activated) to DB75 via a complex pathway involving CYP1A1, 1A2, 3A4, 4F2, 4FB, 2J2 and b5, prior to nuclear binding. Hence, it is suggested that a similar or homologous metabolic pathways exist in medaka. (A) STII medaka, 20 dpf: Widefield fluorescence microscopy, control liver (L) at 45 minutes. (B) STII medaka, 24 dpf: 45 minutes post exposure to DB289 fluorescence of the active metabolite DB75 (confirmed with analytical chemistry) was detected in the liver and gut (Gt). (C) STII medaka, 26 dpf: 24 hours post exposure fluorescence in the gut lumen was markedly increased. (D & E) STII medaka, 26 dpf: Higher magnification image showing DNA binding in hepatocytes 72 hrs post exposure. Red cells can be seen in the lumen of the hepatic vein (Hv/r). (F) STII medaka, 34 dpf: Shown is in vivo image of medaka brain 5 hrs post DB289 exposure. No nuclear binding was observed in the brain up to 10 days of exposure. Optic tectum (Ot), Corpus cerebelli (Ce).

tion in intrahepatic biliary passageways as early as 15 minutes post administration (aqueous bath), the fluorescent ceramide was not observed to accumulate (peak fluorescence) in the hepatobiliary system until ~60 minutes after dosing. Like β -Bodipy HPC, Bodipy FL C5 ceramide appeared to be taken up across gill epithelia, and transported through the cardiovascular system to the liver and gut (Figure 3). Cardiovascular transport of Bodipy FL C5 ceramide was much more distinct than that of Bodipy HPC, with marked labeling of endothelium and red blood cells. Bodipy FL C5 ceramide, because of its apparently slower, passive uptake, and accumulation in the cytosol of virtually all cell types, was found optimal for investigating epithelial cell morphology in vivo.

This fluorophore showed near even distribution within blood plasma, the cytosol, and intrahepatic bile passageways. Hence, Bodipy FL C5 ceramide was the fluorophore of choice for elucidating cell morphology in vivo; allowing imaging of hepatocellular space, biliary space, and vasculature, simultaneously.

In summary, both Bodipy FL C5 Ceramide and β -Bodipy C5-HPC showed differential transport; where Bodipy C5-HPC, an organic cation, exhibited kinetics and differential distribution between blood and bile that suggested active transport, C5 ceramide exhibited slower uptake with an even distribution through the vasculature, hepatocellular, and bile spaces, consistent with passive diffusion of the fluorophore across cell membranes.

Table 2. Endogenous Fluorophores

	Ex (nm)	Em (nm)
Flavoproteins: flavine adenine dinucleotide (FAD), flavin mononucleotide (FMN)	450	550
Pyridine Nucleotides: nicotinamide dinucleotide (NAD), nicotinamide dinucleotide phosphate (NADP). *The reduced states fluoresce – NADPH, NADH	336	450
Tryptophan	295	329
Hydroxykynurenine glucoside (3-HGK)	520	550
Serotonin (5-HT)	290/366	340-440/510
5 HIAA	300	350
α -naphthol	340	460
Bilirubin	435	500
Protoporphyrin	424/408	594/630
Collagen I	340/500	410/520
Elastin	330	405
Lipofuscin	300	420
Vitamin A	345	490
Vitamin E	295	335
Thiamin (B1)	366	430
Riboflavin (B2)	440	514
Salicylic Acid	319	408

Examples of some the known endogenous fluorophores and their excitation/emission wavelengths are listed.

Overall, both probes were found to be efficacious for elucidating biological structure/function *in vivo*, and thereby, morphological changes (e.g. cytotoxicity) in response to xenobiotic exposure (see Figures 3, 6, 8 and 9 for comparison).

The highly lipophilic Bodipy 505/515 and 493, like β -Bodipy C5-HPC, were also found to be excellent fluorophores for investigating hepatobiliary transport and bile secretion (Figure 3). Both probes allowed elucidation of the intrahepatic biliary passageways, extrahepatic biliary passageways, gut lumen, and intestinal lumen (e.g. mucosal folds of the gut).

Perhaps the most utilized probe for elucidating the biliary architecture was the widely employed fluorophore fluorescein isothiocyanate (FITC). This small organic cation showed rapid branchial uptake, with marked differential distribution between blood and bile. Because of the difference in concentration of FITC in blood and bile on a temporal scale, this allowed for high resolution *in vivo* investigation into biliary morphology, bile transport, and xenobiotic response. Examples of the application of FITC to *in vivo* investigations can be seen in Figures 7 & 8.

Several probes were found to be useful for *in vivo* nuclear labeling, these were: DAPI 4',6-diamidino-2-phenylindole, dihydrochloride;

DAPI DiAcetate 4',6-diamidino-2-phenylindole, dilactate; CellTrace Oregon Green 488 carboxylic acid diacetate, succinimidyl ester; and the SYTO[®] series of fluorescent probes from Invitrogen (e.g. SYTO[®] 16 green fluorescent nucleic acid stain).

An additional example of *in vivo* investigation of nucleophilic fluorophores can be seen in preliminary studies examining the absorption, distribution, metabolism and excretion, as well as toxicity (ADME/Tox), of an experimental pro-drug for treatment of trypanosomiasis (Figure 4). Preliminary results with two anti-trypanosomal compounds, termed DB compounds (DB289 and DB75), revealed metabolism of the parent compound, DB289, and nuclear binding of the biologically active fluorescent metabolite, DB75, to gill epithelia and hepatocytes within 15 minutes of exposure. Temporal assessment of distribution and metabolism showed nuclear binding of the metabolite increased with time, peaking at 90 minutes, with distribution expanding to the gut, pancreas and systemic tissues over a 24 hr period. In rodent and primate models DB289 is metabolized via a complex pathway involving CYP1A1, 1A2, 3A4, 4F2, 4FB, 2J2 and b5 (Dr. J.Ed. Hall, UNC Chapel Hill, personal communication). Hence, similar or homologous metabolic pathway(s) likely exist in medaka, though such pathways remain

to be elucidated.

The ability to label and visualize nuclei of individual cells in organs and tissues proved valuable not only for structural elucidation, but for differentiation between nuclei and cellular lesions (described later in the xenobiotic response section), where nuclei were differentiated from hydropic vacuoles. The efficacy of the nuclear labeling fluorophores is illustrated in Figure 4 and 9.

In addition to the utilization of exogenous fluorophores, autofluorescence of live cells also proved useful in delineation of cellular and tissue morphology in vivo. Autofluorescence is an innate property of living cells (*note, we observed the autofluorescence of non viable cells and tissues was diminished relative to their viable counterparts). A variety of endogenous compounds are known to exhibit autofluorescence under a variety of excitation/emission spectra (Table 2). Among these, endogenous fluorescence of nicotinamide adenine dinucleotide phosphate (NADPH), riboflavin, flavin co-enzymes and flavoproteins, as well as porphyrins, are each used as indicators of enzyme activity and physiological state in living cells (Boonacker and Van Noorden 2001). For instance, NADPH fluoresces in its reduced state, but not in its oxidized state (e.g. NADP). In contrast flavin adenine dinucleotide fluoresces in its oxidized state (FAD), while fluorescence is undetectable when reduced to FADH₂. Because each of these endogenous fluorophores is widely employed in a variety of cellular processes, they, by their fluorescence, can be good indicators of cell viability and function. For instance, Ramanujam *et al* (1994) reported that dysplastic cells exhibited greater fluorescence, likely due to increased metabolic rate of altered cell types. From these findings UV light excitation has been used to differentiate neoplastic cervical tissue from normal tissues, in vivo (Ramanujam *et al.* 1994). Similarly, differential fluorescence has been employed to distinguish normal, hyperplastic, and adenomatous human colonic mucosa epithelia cells (primary cell cultures) (DaCosta *et al.* 2005).

Of the endogenous fluorophores, NADPH is a likely candidate for much of the tissue autofluorescence observed in vivo in the findings presented here (where we employed excitation of ~350-400 nm, DAPI/UV). Excitation at this wavelength resulted in autofluorescence in virtually all cell types in medaka. The same has also been reported for mammalian and other piscine species (see

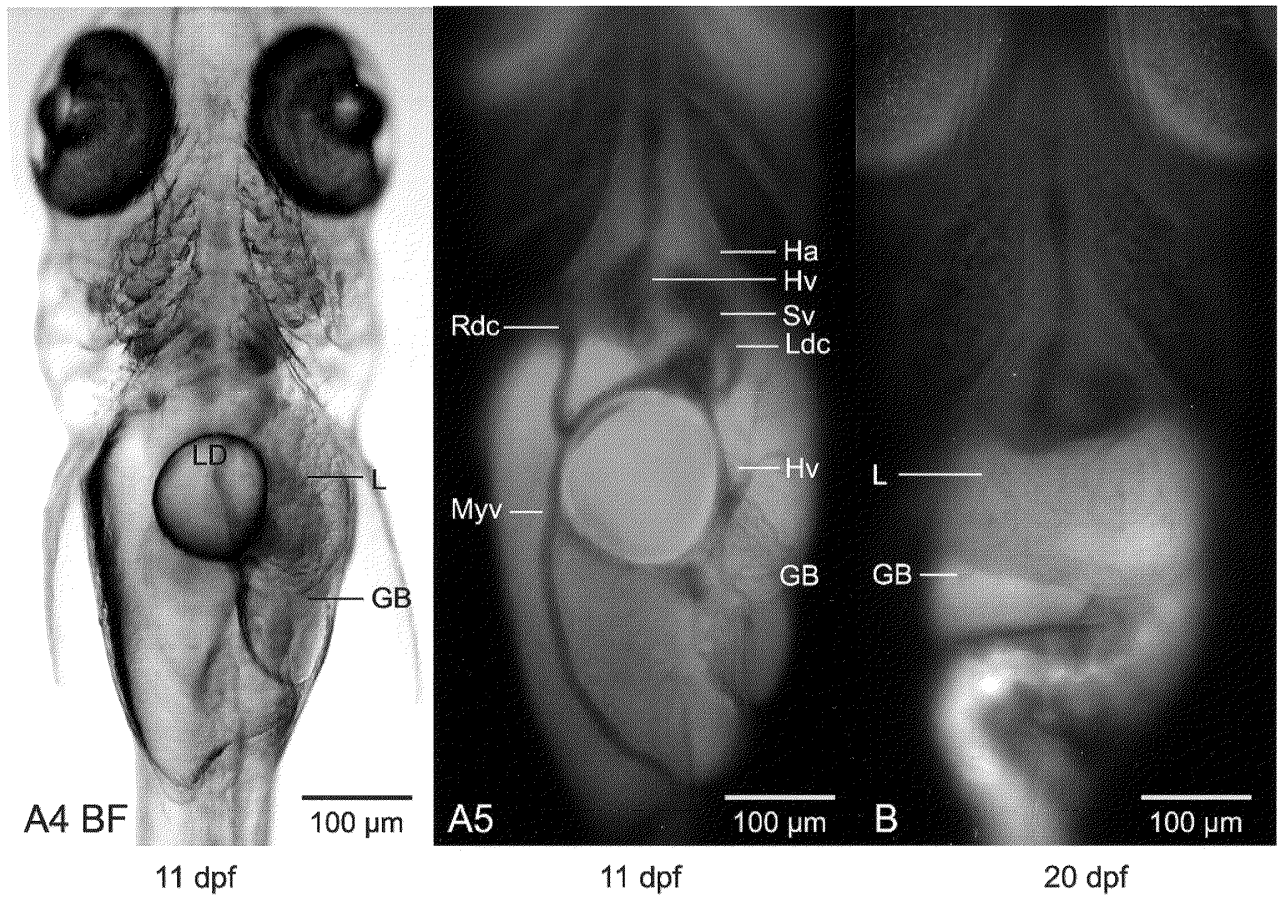
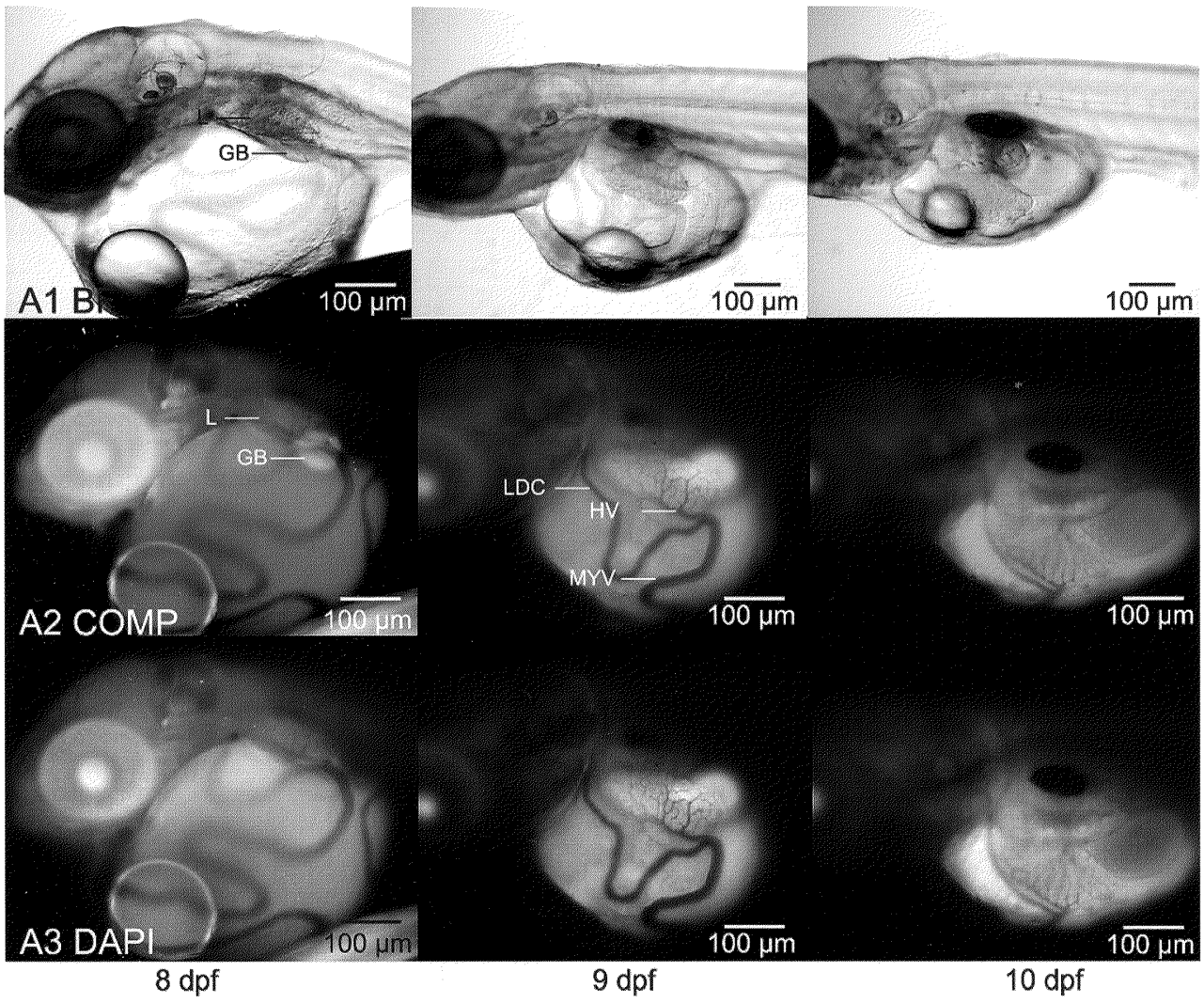
review by Boonacker and Van Noorden, 2001).

While UV/DAPI can be phototoxic to cells, it was at times of value to utilize this excitation wavelength (autofluorescence of tissues) to elucidate morphological features otherwise difficult to visualize. For instance, UV/DAPI excitation was highly useful for visualizing the vasculature of medaka liver, and vasculature throughout the body (blood plasma was relatively non fluorescent compared to individual epithelial, endothelial and red blood cells). UV/DAPI was also useful for visualizing individual cells in vivo (e.g. hepatocyte morphology). Hence, by utilizing the autofluorescence properties of cells/tissues savings in time and materials may be realized, negating the need to administer exogenous fluorophores to elucidate cellular/tissue morphology in vivo.

At other excitation/emission wavelengths (TRITC/FITC) tissue autofluorescence was less distinct, and less widely distributed in cell/tissues, than that observed with DAPI/UV. However, autofluorescence of bile fluid was very distinct under both TRITC & FITC illumination. Because of this TRITC/FITC excitation/emission could be employed to detect the onset of bile synthesis (endogenous bile fluorescence), and to observe bile transport in vivo. Of interest, we observed bile autofluorescence to vary on a temporal scale, a fact which merits further detailed study. While TRITC/FITC excitation resulted in distinct autofluorescence of intra- and extrahepatic bile passageways, as well as gall bladder, it was not consistently observed, suggesting variations in bile composition, perhaps due to varying concentrations of endogenous fluorophores (in bile) previously discussed (e.g. NADP, FADH, porphyrin compounds). For this reason, it was not possible to fully utilize bile autofluorescence alone as an indicator of transport of specific bile constituents.

In vivo description of hepatobiliary development

In vivo observation/imaging permitted detailed study and description of development of the medaka hepatobiliary system. This included observation/description of hallmark events such as organogenesis, the onset of bile synthesis and transport, and metamorphosis of the liver from an embryonic to adult phenotype (Figure 5). The ability to make in vivo investigations at various stages of hepatobiliary development led to important insights (e.g. parenchymal architecture during embryonic, larval and juvenile stages of development) (Hardman *et al.* 2007). While a lengthy dis-



cussion of these events is beyond the scope of the article, Figure 5 provides an overview of results from these studies.

Quantitation of hepatobiliary transport in vivo

Perhaps the more salient examples that best illustrate the utility of in vivo investigation in STII medaka are those that characterized the 3D architecture of the medaka liver, and elucidated hepatobiliary transport and xenobiotic response.

Transport of solutes from blood to bile is a vital liver function. It is through bile synthesis and transport that xenobiotics of environmental origin (e.g. environmental toxicants/toxins, pharmaceuticals), and endogenous metabolic by-products, are either safely removed from the system, or, with systemic accumulation, result in morbidity/mortality. Inhibition/impairment of bile transport (cholestasis) commonly results in morbidity/mortality in mammals, and little is known about bile transport in piscine species and the relationship of impaired transport function in these organisms to disease and toxicity. While it is becoming increasingly apparent that many piscine species share bile synthetic and transport mechanisms with their mammalian counterparts (Hagey 1992; Moschetta *et al.* 2005; Hinton *et al.* 2007), no studies on fish cholestasis in response to disease and toxicity exist.

Our preliminary investigations show in vivo quantitation of hepatobiliary transport in STII medaka is possible. Using fluorescent probes success was achieved in establishing methods for quantifying blood to bile transport in vivo (Figure 6). For accurate quantitation of transport several key elements were necessary. Most of the hurdles to quantitation were found to be digi-

tally based, or rather, lay in microscopy/imaging technologies, rather than limits imposed by the STII animal model itself. For instance, one of the primary issues was standardization of microscopy techniques (Taylor and Wang 1989; Webb *et al.* 1990; St. Croix *et al.* 2005). Exposure times while imaging (e.g. fluorophore quenching), laser intensity (excitation), fluorophore concentration in the exposure bath, and imaging depth in vivo (e.g. how deep into the tissues you are imaging), were all found to influence and define the digital image information captured in vivo, and this, in turn, affected quantitation of digital information. Hence, an important consideration was the type of software used for digital image acquisition and quantitation. This was/is a potential source of error if not well understood. For instance, for some software programs, such as ImageJ, digital image format (whether the digital image was 8, 16 or 32 bit, color or grayscale) potentially affected quantitative analysis. These parameters, pixel depth and color profile, are determined by the image acquisition software (software that interfaces with digital CCD cameras on confocal or widefield microscopes; in this case IP Lab was the software acquisition program for the widefield microscope, Zeiss LSM 5 Axiovision image acquisition software for the confocal microscope). Hence, while digital image acquisition, in our case, occurred in IP Lab and Zeiss LSM 5 Axiovision programs, quantitation was performed using third party software (ImageJ, Zeiss Image Browser 5 and Amira 3D, see materials and methods). Hence, it was often necessary to convert the original image (acquired) to a pixel depth and color profile that was optimal and/or compatible with the quantitation software employed. Perhaps

Figure 5. In vivo investigations of hepatobiliary development. (A1:First Row) Brightfield microscopy. (A2:Second Row) Widefield fluorescence microscopy, DAPI and TRITC composites revealing gall bladder (GB, red) position. (A3:Third Row) Widefield fluorescence microscopy, DAPI autofluorescence elucidating vasculature. At day of hatching, 8 dpf, the liver was found as the L5 phenotype, left lateral and ventral to the 3rd somite (A1-A3 1st column). From 8 to 11 dpf the L5 liver and gall bladder descended to the ventral abdomen, with marked restructuring of the associated vasculature. (A4, A5) Translocation of the L5 liver and gall bladder to the ventral abdomen was characterized by: descent of the liver and GB, which remain in longitudinal position, yolk resorption, the disappearance of the stomatodeal and proctodeal membranes (not shown), the onset of peristalsis, and the beginning of respiration. (A4) Brightfield microscopy, 11 dpf, ventral view, showing liver (L), gall bladder (GB) and lipid droplet (LD). (A5) Widefield fluorescence microscopy, DAPI/TRITC composite, ventral view, elucidating liver, gall bladder and vasculature. The onset of metamorphosis of the hepatobiliary system to a transverse position in the rostral abdominal cavity (adult phenotype) began at 11 dpf. (B) Widefield fluorescence microscopy, DAPI image capture, ventral view. By 20 dpf the liver and gall bladder were transverse in the ventro-rostral abdominal cavity, marking the attainment of the adult phenotype. As can be discerned from the images shown, marked restructuring of the vasculature accompanied metamorphosis of the liver and gall bladder from an embryonic to adult phenotype. While such observations are purely descriptive, they permitted elucidation of hallmark events in hepatobiliary development and helped characterize normalcy in vivo. Liver (L), Gall Bladder (GB), Heart Atrium (Ha), Heart Ventricle (Hv), Sinus Venosus (Sv), Hepatic Vein (Hv), Left Duct of Cuvier (Ldc), Median Yolk Vein (Myv), Lipid Droplet (LD)

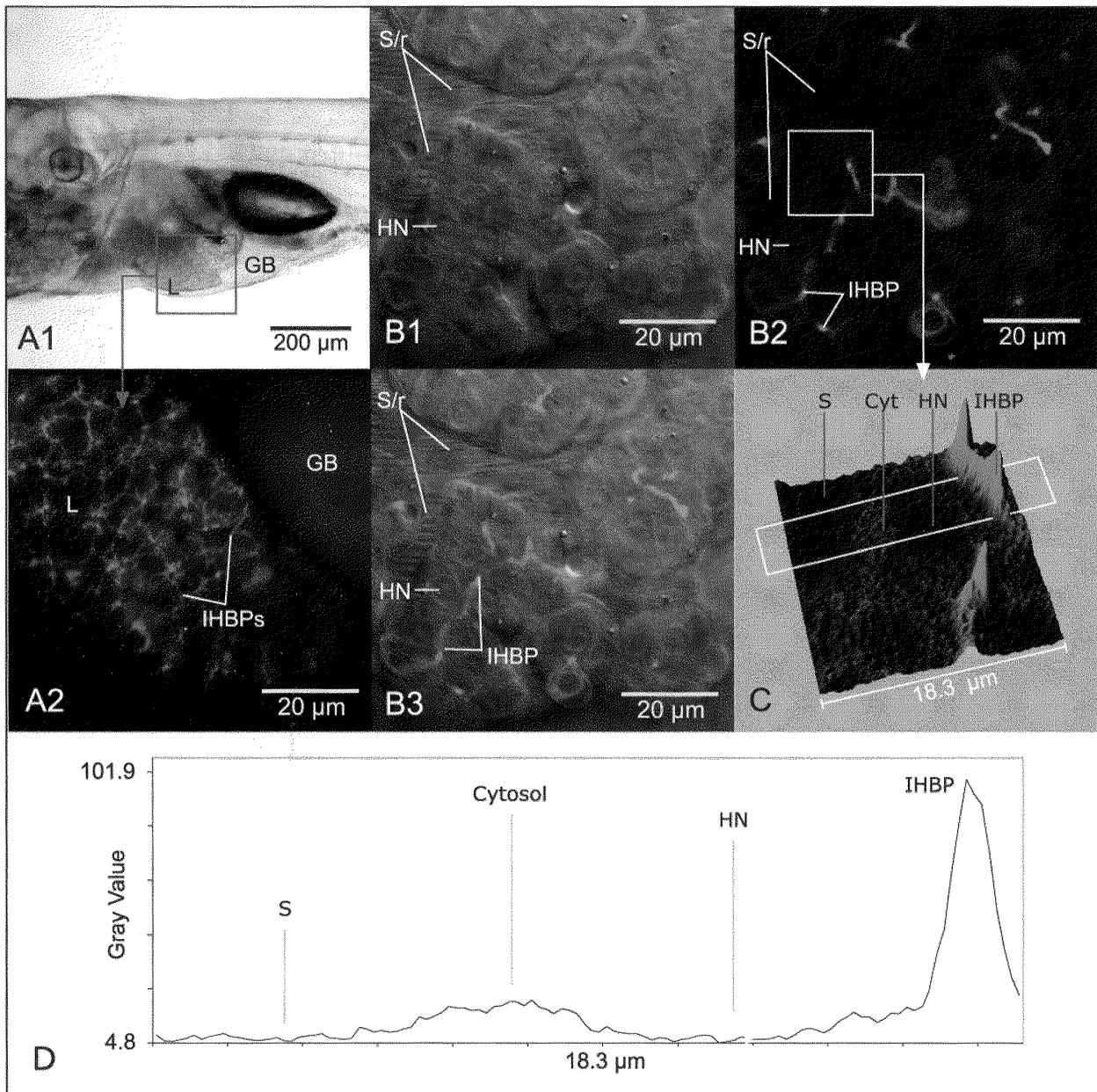
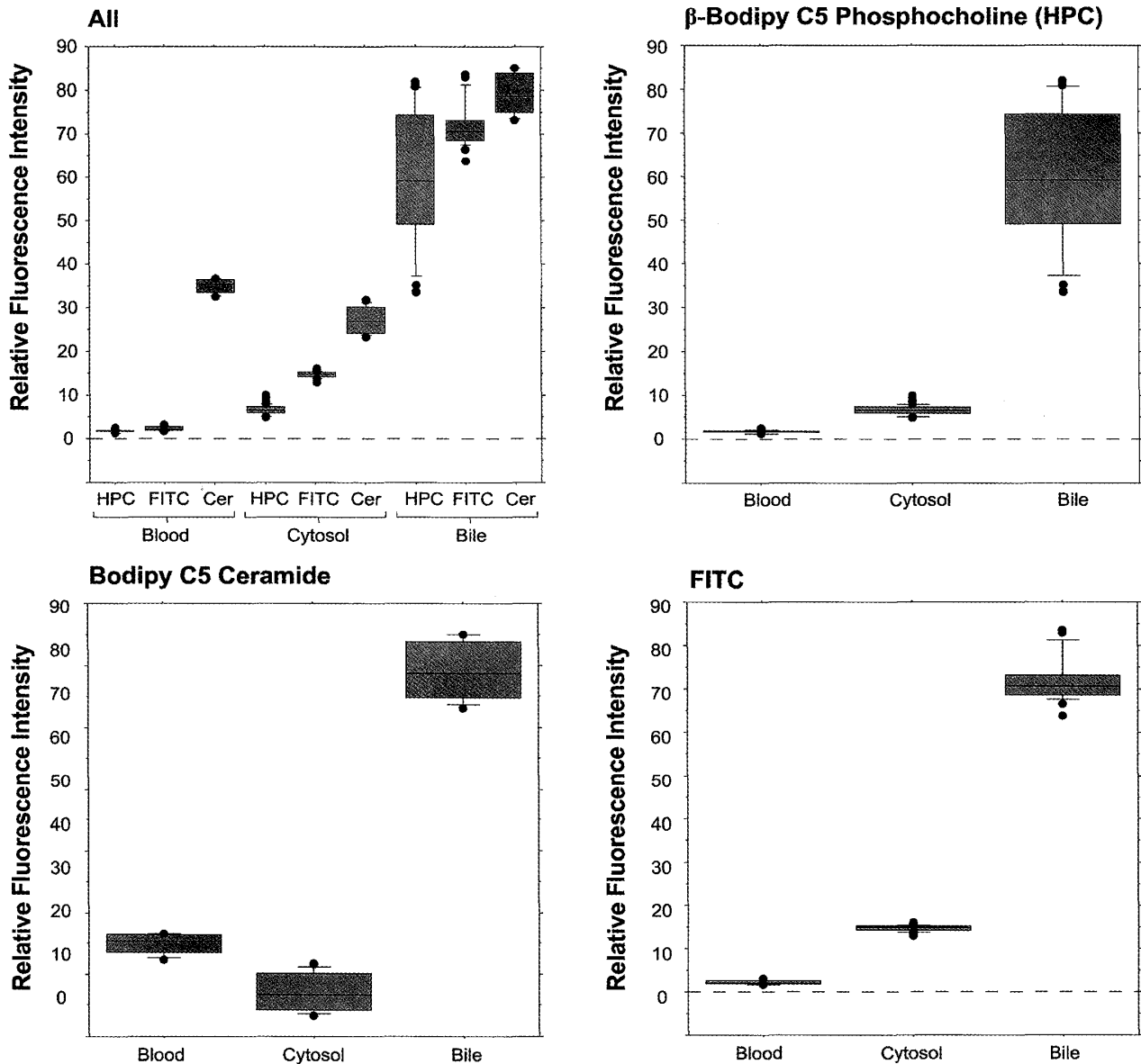


Figure 6. In vivo quantitation of hepatobiliary transport. Fluorophores such as β -Bodipy C5 phosphocholine, shown here, enabled in vivo elucidation of the biliary system and quantitation of blood to bile transport. (A1) Brightfield microscopy of STII medaka at 30 dpf. Green algae can be seen in transport through lumen of the gut. (A2) Widefield fluorescence microscopy of region of interest indicated by gray square in A1, showing β -Bodipy C5 phosphocholine fluorescence in intrahepatic biliary passageways (IHBP) of the liver (L) and gall bladder (GB). (B1) STII medaka, 9 dpf, confocal DIC microscopy. In longitudinal section 2 rows of hepatocytes and their nuclei (HN) characterize parenchymal architecture. Stacked ovate structures are red blood cells in circulation through the sinusoids (S/r). Red cells appear flattened due to active circulation of cells through sinusoids, and resulting distortion during imaging. (B2) Same as B1, single frame from in vivo confocal image stack capturing β -Bodipy C5 phosphocholine (green fluorescence) in transport from blood to bile, through intrahepatic biliary passageways (IHBP) of the liver. The fluorophore was imaged in vivo 30 minutes post administration (aqueous bath). (B3) Composite of frames B1 and B2 localizing fluorophore transport to area between apical membranes of adjacent hepatocytes, suggesting active transport of the fluorophore into IHBPs. (C & D) Frame C is surface map of region of interest (white square) in frame B2, illustrating concentrative transport of the fluorophore from sinusoidal space (S) to bile space (BP). The white rectangular region of interest in frame B2, spanning an 18.3 μm area from blood to bile (sinusoid to canaliculus), was quantitatively assessed (frame D), and suggested β -Bodipy C5 phosphocholine concentration (fluorescence intensity) to be ~ 20 times greater in the biliary passageway (IHBP) than in sinusoidal space (S). Also evident is an increase in cytosolic (Cyt) concentration of the fluorophore, while no fluorescence was detected in the nucleus (HN). These types of studies demonstrated concentrative transport of fluorescent probes from blood to bile can be imaged and quantitatively evaluated in vivo. Also illustrated is the utility of fluorophores such as β -Bodipy C5 phosphocholine in elucidating bile canaliculi, ductules and ducts. Confocal images captured with C-apochromatic objective, 1.2 NA w/correction, 488 nm excitation, Zeiss LSM 510.

Blood to Bile Transport In Vivo: β -Bodipy C5 Phosphocholine (HPC), Bodipy C5 Ceramide, Fluorescein Isothiocyanate (FITC), Area Averages, STII Medaka 12 dpf



F-test: Hypothesized Ratio = 1

	Canalicular		Cytosol		Sinusoid	
	F-value	P-value	F-value	P-value	F-value	P-value
C5 Ceramide: FITC	1.026	0.9665	38.508	<.0001	18.672	0.0001
C5 Ceramide: HPC	0.117	0.0019	17.109	0.0002	28.413	<.0001
FITC:HPC	0.114	<.0001	0.444	0.0686	1.522	0.3412

Figure 7. Quantitative analysis of blood to bile transport in vivo: β -Bodipy C5 phosphocholine (HPC), fluorescein isothiocyanate (FITC) and Bodipy C5 ceramide. Quantitative analysis of differential blood to bile transport between β -Bodipy C5 phosphocholine (HPC), fluorescein isothiocyanate (FITC) and Bodipy C5 ceramide. All fluorophores were imaged in vivo at peak uptake times (Table 1). Differences in blood to bile transport between all three fluorophores are suggested when measured values (means) of fluorescence intensity across sinusoid, cytosol and canalicular spaces were assessed. The most marked differences were between β -Bodipy C5 phosphocholine and fluorescein isothiocyanate, and Bodipy C5 ceramide. This was considered to be due to (based on in vivo observations) active transport of both β -Bodipy C5 phosphocholine and fluorescein isothiocyanate vs. passive transport of Bodipy C5 ceramide. Interestingly, while there was clear concentration of the ceramide fluorophore in the canalculus, transport of the fluorescent ceramide saw decreased fluorescence intensity in the cytosol, as compared to both sinusoid and canalculus. Equality of variance F-test comparing measured values (repeated measures, which varied from 30 to 70 depending on number of stacks and available fields) in cytosol, sinusoid and canalicular spaces are given with P-values.

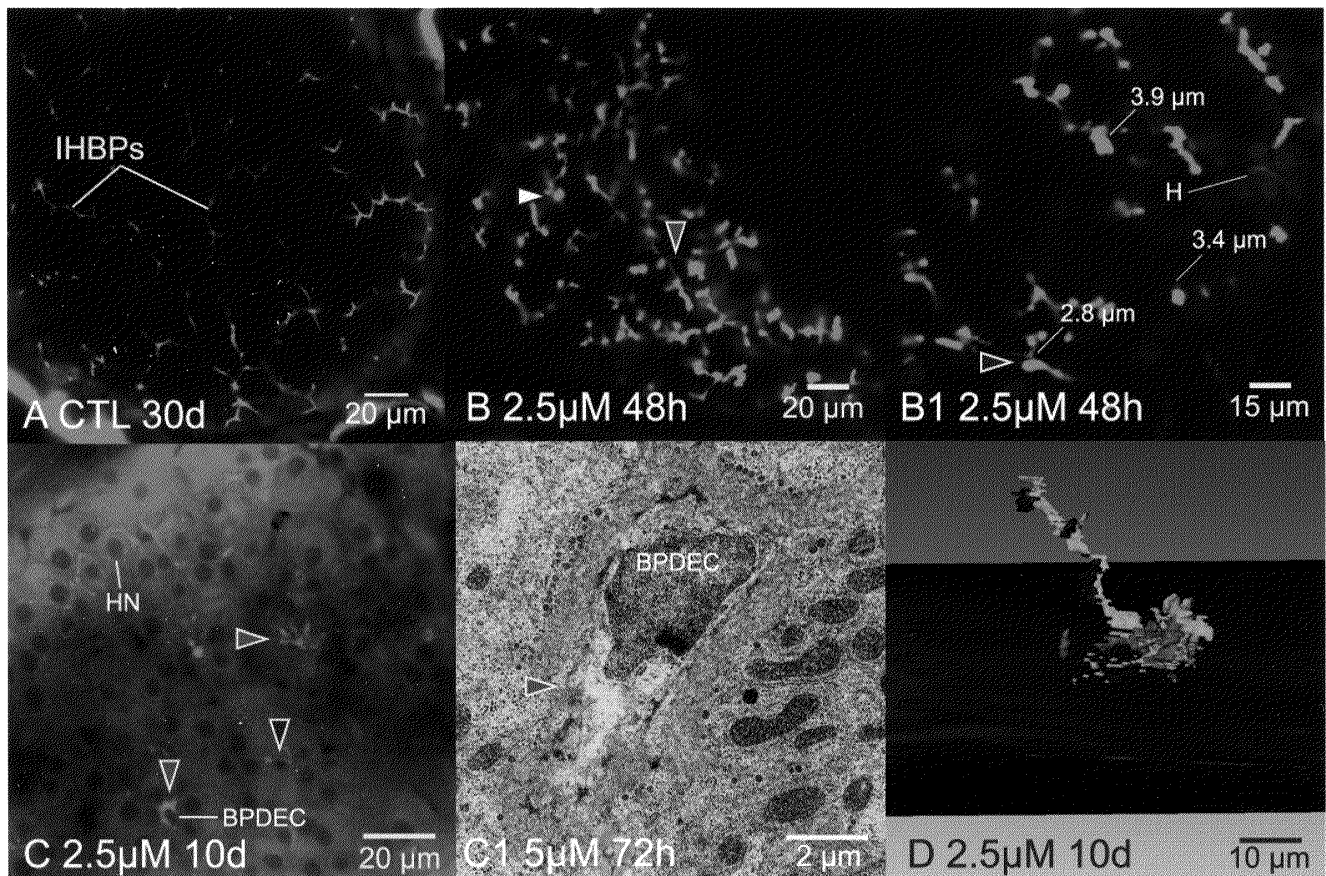


Figure 8. In vivo imaging of hepatobiliary response to ANIT exposure: canalicular attenuation & dilation. (A) In vivo confocal image of untreated medaka liver (30 dpf), note uniformity of diameter of IHBPs. (B-B1) In vivo confocal image of ANIT treated medaka liver (24 dpf) showing dilated and attenuated bile canaliculi (red arrowhead points to attenuation, white to dilation) at 48 hrs post exposure to 2.5 μM ANIT. Only the intrahepatic biliary passageways are fluorescent (FITC, green). Parenchyma is largely non fluorescent, aside from weak and diffuse fluorescence of hepatocellular cytosol. (B1) Dilated canaliculi (black arrowhead; elucidated with FITC) were found to be up to approximately 3 times normal diameter (e.g. 3.9 μm diameter in dilated vs. 1.3 μm average diameter in normal canaliculi). Attenuated canaliculi were distinct, appearing as fine sinuous passageways measuring 0.4 μm to 0.8 μm in diameter (*canalicular attenuation/dilation was not readily apparent in histological and ultrastructural studies). (C) Non invasive in vivo confocal image 10 days post exposure to 2.5 μM ANIT (chronic exposure) illustrating bile productular lesions (red arrowheads), characterized by loss of productule membrane integrity and loss of uniformity in lumen diameter. Intrahepatic biliary passageways elucidated here with Bodipy C5 Ceramide. Black arrowhead illustrates appearance of normal bile productule. (C1) Transmission electron micrograph illustrating changes to bile productular epithelia (BPDEC) associated with productular lesions, which showed increased cytosolic area and vacuolation (red arrowhead). In vivo observations helped lead to the hypothesis that ANIT induced BPDEC toxicity is responsible for bile productular lesions observed, and that these cells are early targets of ANIT toxicity, with hepatocellular responses observed subsequent to BPDEC response. (D) Example of 3D reconstruction of damaged productule reveals the damaged bile passageway (green) was blind ending, not interconnected with other segments of the intrahepatic biliary network. Also shown are bile productular epithelial cells (purple), suggesting the damaged area was a canaliculo-productular junction. In (A, B, B1) IHBPs elucidated with FITC, in (C) with Bodipy C5 ceramide.

one of the most important factors was the temporal scale of study, or the time of image acquisition. Most fluorophores used for investigation of blood to bile transport were observed to be assimilated by medaka fairly rapidly (15–20 minutes for initial uptake from aqueous bath). Peak uptake (or saturation), occurred some 15 to 90 minutes later, depending on the fluorophore used (Table 1).

Hence, in developing in vivo methodology for quantifying hepatobiliary transport, several key elements were/are required. First, uptake, distribution and transport of individual fluorophores

should need full characterization for standardization of protocols. This entails characterizing temporal changes, as well as the effect of fluorophore concentration (aqueous bath) on uptake and transport dynamics/kinetics. In our investigations rigorous study and thorough determination of fluorophore dynamics/kinetics in vivo was not possible due to the lack of a dedicated confocal instrument, and time. In lieu of this type of characterization, peak uptake times, and a time frame subsequent to peak uptake time that allows for in vivo imaging and quantitation of transport, was determined for

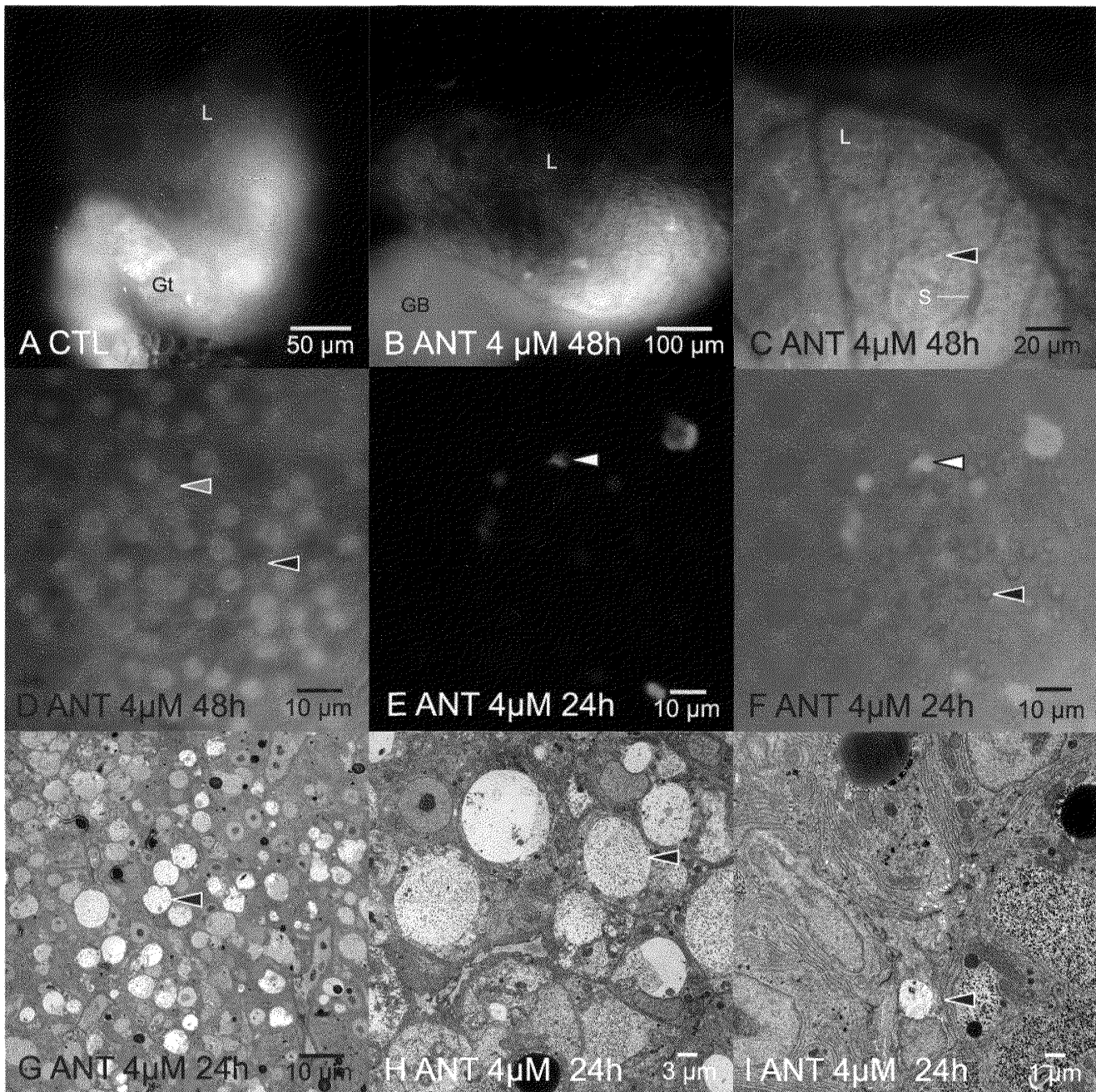


Figure 9. In vivo imaging of hepatobiliary response to ANIT exposure: hydroptic vacuolation. ANIT concentrations (aqueous bath exposures) of 2 to 8 μM resulted in a marked “pebbling” of the liver. This terminology was used due to morphological appearance of the liver, first observed in vivo with widefield fluorescence microscopy. (A) STII medaka control, 16 dpf, showing the normal smooth appearance of the parenchyma in vivo as viewed with widefield fluorescence microscopy at 24 hrs. Liver (L), Gut (Gt). (B&C) STII medaka, 20 dpf, widefield fluorescence FITC image captures illustrating the distinct parenchymal pebbling in response to ANIT. Non invasive in vivo imaging elucidated what appeared to be ovate structures within the cytosol of hepatocytes, giving a pebbled appearance to the plane of focus in the liver. This phenotype was observed with the aid of auto-fluorescence alone (DPAP/UV, TRITC), no fluorophores were necessary for visualizing this cellular response. Gall bladder (GB, Sinusoid (S). (D) ANIT exposed medaka were simultaneously treated with the nuclear stain DAPI (aqueous bath) to label hepatocyte and biliary epithelial cell nuclei. After 1 hr of DAPI exposure the hepatobiliary systems of medaka were imaged in vivo via widefield fluorescence microscopy. These investigations revealed intracellular ovate structures (black arrowhead) did not label with DAPI, and were distinguishable from hepatic and biliary epithelial nuclei (gray arrowhead). (E&F) Experiments investigating apoptosis were performed with YO-PRO-1, a nucleic acid stain. Image E shows uptake of YO-PRO-1 into cells with compromised cell membranes. (F) In vivo confocal image of YO-PRO-1, a DIC and TRITC composite. In the grayscale DIC image hydroptic vacuoles (black arrowhead) are readily apparent. Associated with hydroptic vacuolation was a slight increase in apoptosis, suggested by green fluorescence of YO-PRO-1 (cell type not known). (G) Semi-thin section (toluidine blue) showing hydroptic vacuolation (black arrowhead) at 24 hrs, 4 μM ANIT dose. Numerous vacuoles are present in a single field. (H & I) Transmission electron micrographs further elucidated hydroptic vacuoles in both hepatocytes (black arrowhead, H) and bile ductular epithelia (black arrowhead, I). Vacuoles ranged from 2 to 10 μm in diameter and were found to be partially to completely filled with electron dense cellular infiltrate.

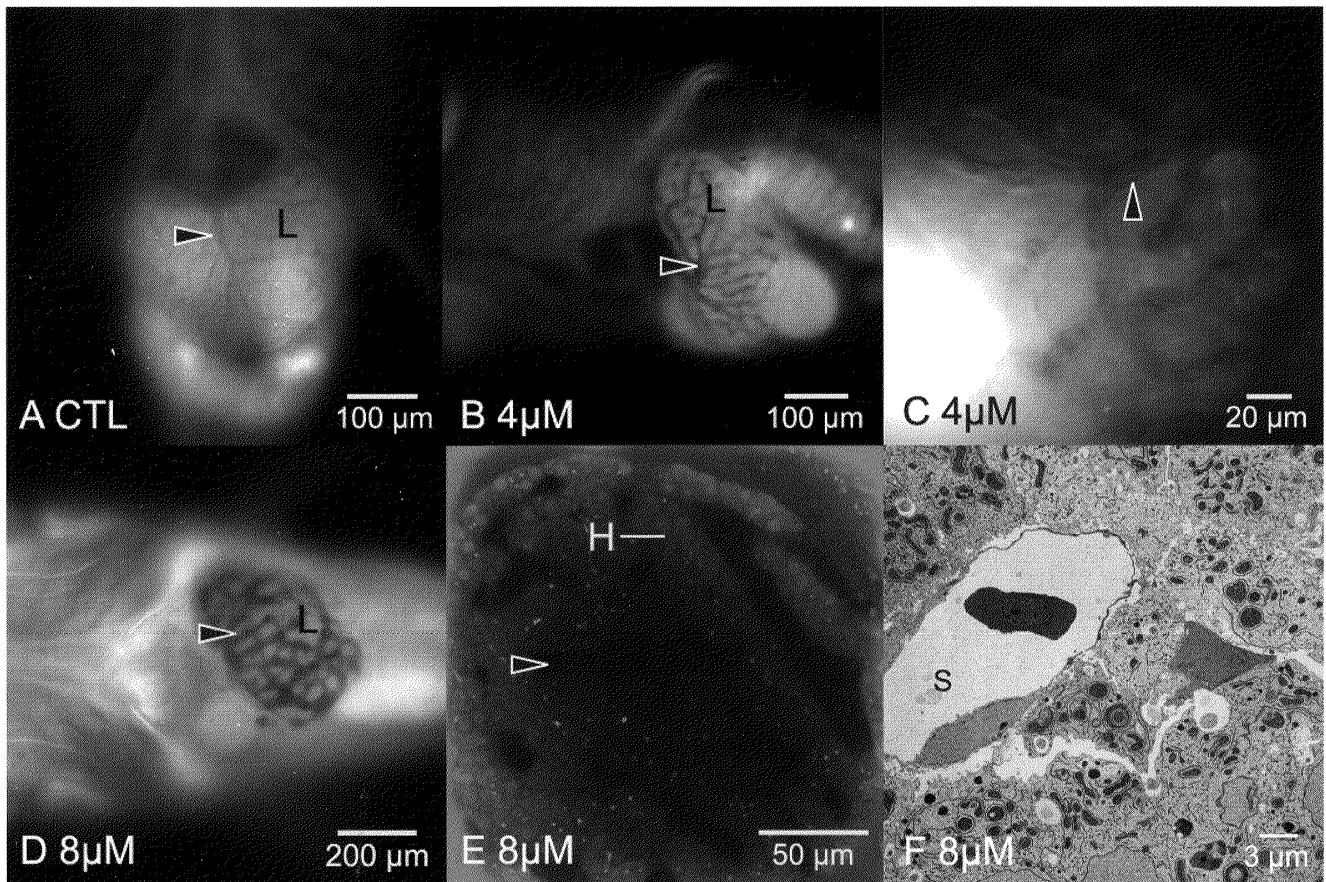


Figure 10. In vivo imaging of hepatobiliary response to ANIT exposure: passive hepatic congestion. (A) Widefield fluorescence DAPI/UV, control liver (L), 20 dpf, 24 hrs post ANIT exposure, showing the normal in vivo appearance of hepatic vasculature (black arrowhead). Hepatic vasculature appears dark (non fluorescent). Epithelia of parenchyma appears light gray. (B & C) At 4 μM ANIT, 24 hrs post exposure, modest dilation of hepatic vasculature (black arrowhead) was observed throughout the liver, as early as 6 hrs post exposure. Image B is DAPI/UV (autofluorescence), image C is TRITC (autofluorescence). (D) At 8 μM ANIT, 24hrs, marked dilation of the intrahepatic vasculature was observed (DAPI/UV). (E) In vivo confocal imaging, acquired at 48 hrs post ANIT exposure, confirmed dilation of intrahepatic vasculature (black arrowhead) was a pan-hepatic response, occurring uniformly throughout the liver. Vasculature is dark gray, hepatocytes and their nuclei fluoresce green. (F) Transmission electron micrograph (8 μM , 20 dpf, 48 hrs post exposure) of an intrahepatic vessel in ANIT treated medaka, revealing abnormal sinusoid/endothelial cell morphology (S). A single red blood cell can be seen in the sinusoid lumen. Endothelium is highly attenuated. In tandem with morphological changes were changes to cardiovascular function; decreasing heart rate and motility along with increase in vasodilation, in medaka exposed to 0.5 μM to 8 μM ANIT, was observed.

each fluorophore employed. We provide in Table 1 times at which fluorescence was first observed in the biliary passageways of the liver (uptake), and the time when fluorescence peaked (saturation). After peak fluorescence was achieved, fluorescence (fluorophore concentration in vivo) was assumed to be at a steady state as long as medaka remained under constant exposure to the fluorophore in aqueous medium. At this point, transport kinetics were assumed to have reached equilibrium (at the exposure concentrations given).

For these studies, it was decided that image acquisition would occur during the time frame that sees initial maximal uptake (saturation), or the time when fluorescence intensity peaks at a given exposure concentration, and for a predefined period of time following the onset of peak fluo-

rescence, determined prior to study. These characteristics were found to be unique for each fluorophore. Hence, in these studies, in vivo imaging was done at the onset peak fluorescence and for, on average, no more than 30 minutes post peak fluorescence.

Lastly, quantitation is based on a measure of fluorescence intensity, the units of which can vary depending on pixel depth and color profile (e.g. brightness, saturation, grayscale value). Hence, there are multiple variables (potentially confounding factors) that need to be controlled for in order to accurately quantify transport of exogenously-administered fluorophores in vivo.

With the above factors accounted for, preliminary findings on quantitation of in vivo transport suggest quantitation of hepatobiliary transport in

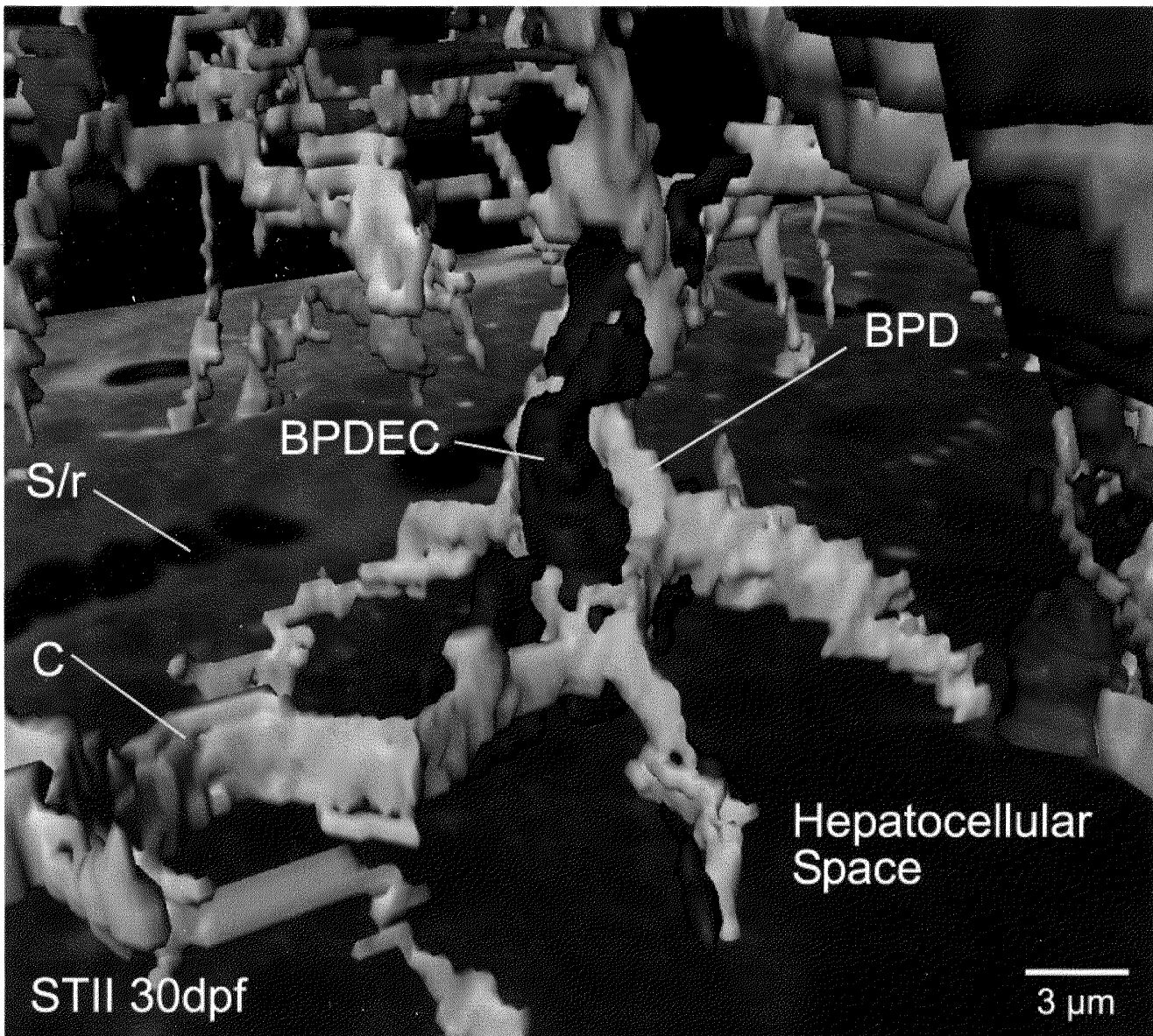


Figure 11. Example of 3D reconstruction of hepatic parenchyma from in vivo confocal image stack: bile productules and productular epithelial cells. Shown is an isolated section of the parenchyma showing the 3D characteristics of bile productular epithelia (BPDEC) and bile productules (BPD), the latter a unique morphological feature created by junctional complexes between BPDECs and hepatocytes. Hepatocytes, which occupy the negative/empty space, are not rendered for visual clarity. A canaliculus (C) is shown joining a bile productule. The background grayscale image is a single frame from a confocal image stack. Red blood cells are seen captured in circulation through sinusoids of the liver (S/r). To our knowledge this was the first rendering of this junctional complex (bile productule) in 3 dimensions, the evaluation which provided novel insights into parenchymal organization.

STII medaka is possible. For instance, empirical observations suggested differential uptake and transport dynamics/kinetics between β -Bodipy C5-HPC, Bodipy C5 Ceramide and fluorescein isothiocyanate. For quantitation, digital image captures from in vivo investigations were converted to both RGB 32 bit color, and 8 bit grayscale. These were then analyzed in ImageJ using the following techniques: regions of interest (ROIs) were defined for sinusoid lumen, hepatocyte cytosol, and canalicular/bile productular lumens. ROIs were measured for fluorescence

intensity (brightness value) in both RGB 32 bit color, and 8 bit grayscale images. In any given image multiple ROIs were randomly selected, for; sinusoidal space, cytosol space and bile space. For instance, in a single confocal stack multiple ROIs were measured in each of the three compartments, resulting in repeated measures. These values (fluorescence intensity), as well as the total area measured for sinusoid, cytosol and bile space, were imported to MS Excel and Statview for statistical analyses. Means were taken for each set of measures (sinusoid, cytosol, bile space) and used

for plots/graphs. Descriptive statistics as well as bivariate analyses were used for quantitation of blood to bile transport. While differences between Bodipy C5 ceramide, and β -Bodipy C5-HPC and fluorescein isothiocyanate were expected, the more subtle, statistically significant differences between β -Bodipy C5-HPC and fluorescein isothiocyanate (Figure 7) were especially interesting. In contrast to C5 ceramide, which exhibits kinetics more consistent with passive diffusion across cell membranes, the latter two fluorophores exhibited kinetics more consistent with active transport. That these differences are putatively indicated here in quantitative results is promising for future investigations into quantifying transport of solutes from blood to bile *in vivo*.

3 Dimensional hepatobiliary architecture: *in vivo* studies

Non invasive *in vivo* imaging allowed the generation of 3D models of the medaka hepatobiliary system. Using confocal fluorescence microscopy (LSCM), in tandem with exogenous fluorophores, we were able to elucidate hepatocellular, biliary and vascular components of the liver. Briefly; the fluorescent probes 7-benzyloxyresorufin (7-BR), Bodipy C5-HPC, Bodipy FL C5-ceramide, DAPI, and fluorescein isothiocyanate (FITC) were administered to living STII medaka in aqueous bath to elucidate specific elements of the hepatobiliary system (e.g. hepatocytes, endothelial cells, biliary epithelia, bile passageways). Individual medaka were exposed to fluorophores (aqueous bath) at the following concentrations and durations: 7-BR (10–50 μ M, 10 to 30 minutes), Bodipy C5-HPC (30 nM–10 μ M, 10 to 30 minutes), Bodipy FL C5-ceramide (500 nM–5 μ M, 10 to 44 minutes), FITC (1 nM–50 μ M, 10 to 30 minutes). After 15–45 minutes of fluorophore exposure STII medaka were sedated, mounted on depression well glass slides with cover slip and imaged live using confocal fluorescence microscopy (LSCM), at various stages of development (8–60 dpf).

Confocal stacks from *in vivo* imaging of the hepatobiliary system were then imported into the 3D rendering and analytical software, Amira 3D. Confocal stacks were comprised of 0.5 μ m to 2 μ m sections (space between individual images/scans), though 0.5 was most commonly employed. Stacks were typically 90 to 120 μ m thick (depth of scan), though in some instances these were combined to create stacks of up to 200 μ m in thickness. 3D reconstructions were then used for archi-

tectural, morphometric and volumetric analyses.

3D analyses yielded important insights, which may not have been possible using standard 2 dimensional histological and ultrastructural methodologies alone (Hardman *et al.* 2007). For instance, 3D analyses revealed that: (1) the hepatic parenchyma is organized as a hexagonal structural motif (polyhedral tessellation), evident in the fine structure of the biliary system; (2) the biliary system is an interconnected network of canaliculi and bile preductules that perfuses the majority of the liver corpus (~95%) uniformly, with equidiameter intrahepatic biliary passageways (IHBP) (1–2 μ m) observed throughout the liver; (3) larger bile ductules and ducts were observed only at the liver hilus, and consequently an arborizing biliary tree was absent, seen only in the rudimentary branching of intrahepatic ducts from the hepatic duct; (4) parenchymal architecture is a predominantly 2 cell thick muralium, though tubule-like formations may also comprise the muralium; (5) the livers of these small fish are replete with BPDECs, the putative mammalian corollary of bipotential progenitor/stem cells; (6) BPDECs and hepatocytes form unique junctional complexes that create bile passageways (bile pre-ductules). The latter findings were of particular interest given importance of these cell types, and were made possible by 3D investigation of BPDEC-hepatocyte junctional complexes. By example; when exposed to the complete carcinogen diethylnitrosamine (DEN), hepatocytes and biliary epithelial cells give rise to tumors of the medaka liver (Okihira and Hinton 1999). Both partial hepatectomy and bile duct ligation followed by high resolution light and electron microscopic findings in trout (Okihira and Hinton 2000) have shown small diameter biliary epithelial cells that form junctional complexes with hepatocytes. Furthermore, the cells lining portions of the intrahepatic biliary system between canaliculi and biliary ductules/ducts proliferate as response to bile duct ligation or partial hepatectomy. These cells, termed bile preductular epithelial cells (BPDECs) (Hampton *et al.* 1988; Hampton *et al.* 1989), may be the teleost equivalent of mammalian oval cells (Golding *et al.* 1996; Fausto and Campbell 2003). Due to their small size, these cells are not easily seen in survey light micrographs of medaka liver. By coupling this transparent organism with specific fluorophores, we are able to “see inside” living organisms to record normal structure and toxic alterations. Examination of 3D models revealed

BPDECs to occupy the center of unique morphological formations created by bile preductular epithelial cells and hepatocytes (Figure 11).

Findings from 3 dimensional studies also suggest the hepatobiliary system in medaka can be, as a conceptual model, considered a single functional unit of the vertebrate liver, akin to individual unit of the mammalian lobule (Hardman *et al.* 2007). While our focus was the hepatobiliary system, it should be evident from the findings presented here and previously (Hardman *et al.* 2007) that these types of investigations (3D) in other organ systems, using the same or similar methodologies, is possible.

In vivo investigation xenobiotic response

Because the ability to investigate xenobiotic response in vivo is one of the most valuable features of the STII medaka animal model, and imaging at the cellular level had not been described, characterization of normalcy (in vivo structure/function) was essential. This was accomplished by describing the in vivo phenotypes of individual cells/tissues (e.g. hepatocytes, biliary epithelia, endothelium) of the hepatobiliary and related organ systems, and 3D structure of the hepatic parenchyma. With normalcy characterized we were then able to apply this experimental system to investigate toxicity in vivo. To do so we used the reference hepatotoxicants α -naphthylisothiocyanate (ANIT), and diethylnitrosamine (DEN). ANIT has been employed in rodent studies to investigate biliary toxicity including cholestasis and arborization of finer diameter passageways (Masyuk *et al.* 2003; Palmeira and Rolo 2004; Ferreira *et al.* 2005). DEN has been widely employed to investigate neoplastic response (Ishikawa and Takayama 1979; Teh 1993; Okihiro and Hinton 1999). In vivo investigations (responses to xenobiotic exposure) were correlated with histopathology, ultrastructure and immunohistochemistry for validation of xenobiotic response/toxicity. An example of non invasive in vivo serial analysis of the adult consequence of early life stage exposure to DEN is given in Figure 1. Shown is an in vivo assessment of neoplastic response of the liver 10 months post exposure to DEN. Histopathology revealed the tumor to be comprised of mixed neoplasms of hepatocellular and biliary origin, and with foci of biliary hyperplasia..

In vivo examinations of responses of the liver to ANIT exposure revealed distinct dose

dependent phenotypic changes. By example: acute exposures to 1-3 μ M ANIT (aqueous bath) resulted in canalicular attenuation and dilation while chronic exposures to 1-5 μ M ANIT resulted in bile preductular lesions. Lesions appeared, in vivo, as markedly dilated (up to 6 μ m) and dysmorphic canaliculi/bile preductules, suggesting loss of hepatocellular/bile preductule membrane integrity (Figure 8). ANIT concentrations of 3-6 μ M resulted in a “pebbling” phenotype, the result of hydropic vacuolation of hepatocytes and biliary epithelial cells (Figure 9). Aqueous ANIT concentrations of 6 μ M to 8 μ M resulted in a phenotypic changes consistent with passive hepatic congestion. In vivo investigations revealed a marked cardiovascular response, where all liver vasculature, both afferent and efferent vessel and sinusoids, showed increasing dilatory response to increasing concentrations of ANIT (Figure 10). This response was observed under both acute and chronic exposure regimes. In tandem with vasodilation of hepatic vasculature, was a concomitant dose dependent decrease in heart rate and motility. Hence, the magnitude of both the vasodilation and heart rate responses were dose dependent, and appeared to be coupled.

Summary

We have presented here the development and application of non invasive in vivo methodologies to the study of biological structure, function and xenobiotic response in STII medaka. The development of this in vivo investigatory “system” encompassed the validation of 23 fluorescent probes for in vivo use in STII medaka, and showed for the first time the application of fluorescent probes to in vivo study of cells and tissues in STII medaka. With confocal microscopy, high resolution (< 1 μ m) in vivo imaging was achieved, permitting full observation of intracellular vesicular trafficking of fluorophores such as Bodipy FL C5 Ceramide. With an expanding array of molecular probes coming available, including quantum dots, STII medaka hold significant potential for future in vivo study. The findings presented here also suggest that in vivo quantitation of hepatobiliary transport is possible. While transport studies are preliminary, these findings show STII medaka provide a unique and invaluable model organism to investigate hepatobiliary transport in piscine species.

Lastly, and significantly, is the ability to investigate biological structure/function relationships,

and xenobiotic response, in 3D. While work over the last decade has markedly advanced high resolution 3D elucidation of structure/function relationships at the molecular and protein levels of biological organization, similar information on organ system structure and function at the cellular level has lagged. The ability to elucidate biological structure/function relationships in a 3D context is invaluable to: (1) advance our interpretive/diagnostic understanding of normalcy and disease in cells, tissues and organs, (2) further our comparative understanding of organ system ontogeny/structure/function, and (3) integrate genetic and molecular information with system levels of biological organization. The latter is particularly important, as one of the main challenges over the next several decades will be the integration and interpretation of subcellular information (e.g. genomic, proteomic, metabolomic) in relation to the complex physiological system in which “omic” mechanisms operate. As these findings suggest, STII medaka provide a unique means by which to integrate mechanism of toxicity (e.g. genomic, proteomic information) with physiological system level responses and phenotypic changes *in vivo* (the overarching goal of our laboratory). While our focus has been the hepatobiliary system, other organ systems are equally amenable to *in vivo* study, and we regard the potential for discovery, within the context of *in vivo* investigation in STII medaka, as significant.

Acknowledgments

Thanks to Dr. David Miller, Laboratory of Pharmacology and Chemistry, National Institute of Environmental Health Sciences, Research Triangle Park, for providing access to their laser scanning confocal microscopy facility, and to the Duke University Integrated Toxicology Program. This publication was made possible by Grant Number 1 RO1 RR018583-02 from the National Center for Research Resources (NCRR), a component of the National Institutes of Health (NIH), and Grant Number R21CA106084-01A1 from the National Cancer Institute (NCI), also a component of NIH. Its contents are solely the responsibility of the authors and do not necessarily represent the official views of NCRR or NIH.

References

- Boonacker, E and Van Noorden, CJ. 2001. Enzyme cytochemical techniques for metabolic mapping in living cells, with special ref-

erence to proteolysis. *J Histochem Cytochem* **49**(12): 1473–86.

DaCosta, RS, Andersson, H, Cirocco, M, Marcon, NE and Wilson, BC. 2005. Autofluorescence characterisation of isolated whole crypts and primary cultured human epithelial cells from normal, hyperplastic, and adenomatous colonic mucosa. *J Clin Pathol* **58**(7): 766–74.

Fausto, N and Campbell, JS. 2003. The role of hepatocytes and oval cells in liver regeneration and repopulation. *Mech Dev* **120**(1): 117–30.

Ferreira, M, Coxito, PM, Sardao, VA, Palmeira, CM and Oliveira, PJ. 2005. Bile acids are toxic for isolated cardiac mitochondria: a possible cause for hepatic-derived cardiomyopathies? *Cardiovasc Toxicol* **5**(1): 63–73.

Golding, M, Sarraf, C, Lalani, EN and Alison, MR. 1996. Reactive biliary epithelium: the product of a pluripotential stem cell compartment? *Hum Pathol* **27**(9): 872–84.

Hagey, L (1992). Bile Acid Biodiversity in Vertebrates: Chemistry and Evolutionary Implication. PhD Dissertation., University of California, San Diego.

Hampton, J, Lantz, R, Goldblatt, P, Lauren, D and Hinton, D. 1988. Functional units in rainbow trout (*Salmo gairdneri*, Richardson) liver: II. The biliary system. *Anat Rec.* **221**(2): 619–634.

Hampton, JA, Lantz, RC and Hinton, DE. 1989. Functional units in rainbow trout (*Salmo gairdneri*, Richardson) liver: III. Morphometric analysis of parenchyma, stroma, and component cell types. *Am J Anat* **185**(1): 58–73.

Hardman, R, Volz, D, Kullman, S and Hinton, DE. 2007. An *In Vivo* Look at Vertebrate Liver Architecture: 3 Dimensional Reconstructions from Medaka (*Oryzias latipes*). *Anatomical Rec.* **290**(7): 770–82.

Hinton, D.E., Segner, H., Au, D.H.T.W., Kullman, S.K., and Hardman, R. Chapter 7. The Liver. In: *The Toxicology of Fishes. Unit 2. Key Target Systems and Organismal Effects.* DiGiulio, R.T. and Hinton, D.E. (eds.) Taylor Press. 2007.

Horning, W and Weber, C (1985). Short-term methods for estimating the chronic toxicity of effluents and receiving waters to freshwater organisms., USEPA (EPA/600/4-85/014): 58–75.

Ishikawa, T and Takayama, S. 1979. Importance of hepatic neoplasms in lower vertebrate animals as a tool in cancer research. *J Toxicol*

- Environ Health* **5**(2-3): 537–50.
- Kashiwada, S, Goka, K, Shiraishi, H, Arizono, K, Ozato, K, Wakamatsu, Y, *et al.* 2007. Age-dependent in situ hepatic and gill CYP1A activity in the see-through medaka (*Oryzias latipes*). *Comparative Biochemistry and Physiology Part C: Toxicology & Pharmacology* **145**(1): 96.
- Masyuk, TV, Ritman, EL and LaRusso, NF. 2003. Hepatic artery and portal vein remodeling in rat liver: vascular response to selective cholangiocyte proliferation. *Am J Pathol* **162**(4): 1175–82.
- Meyer, JN, Nacci, DE and Di Giulio, RT. 2002. Cytochrome P4501A (CYP1A) in killifish (*Fundulus heteroclitus*): heritability of altered expression and relationship to survival in contaminated sediments. *Toxicol Sci* **68**(1): 69–81.
- Moschetta, A, Xu, F, Hagey, LR, van Berge-Henegouwen, GP, van Erpecum, KJ, Brouwers, JF, *et al.* 2005. A phylogenetic survey of biliary lipids in vertebrates. *J. Lipid Res.* **46**(10): 2221–2232.
- Nacci, DE, Kohan, M, Pelletier, M and George, E. 2002. Effects of benzo[a]pyrene exposure on a fish population resistant to the toxic effects of dioxin-like compounds. *Aquatic Toxicology* **57**(4): 203.
- Okihiro, M and Hinton, D. 1999. Progression of hepatic neoplasia in medaka (*Oryzias latipes*) exposed to diethylnitrosamine. *Carcinogenesis* **20**(6): 933–40.
- Okihiro, MS and Hinton, DE. 2000. Partial hepatectomy and bile duct ligation in rainbow trout (*Oncorhynchus mykiss*): histologic, immunohistochemical and enzyme histochemical characterization of hepatic regeneration and biliary hyperplasia. *Toxicol Pathol* **28**(2): 342–56.
- Palmeira, CM and Rolo, AP. 2004. Mitochondrially-mediated toxicity of bile acids. *Toxicology* **203**(1-3): 1–15.
- Ramanujam, N, Mitchell, MF, Mahadevan, A, Thomsen, S, Silva, E and Richards-Kortum, R. 1994. Fluorescence spectroscopy: a diagnostic tool for cervical intraepithelial neoplasia (CIN). *Gynecol Oncol* **52**(1): 31–8.
- St. Croix, C, Shand, S and Watkins, S. 2005. Confocal microscopy; comparisons, applications and problems. *Biotechniques* 39.
- Taylor, D and Wang, Y 1989. *Methods in Cell Biology: Fluorescence Microscopy of Living Cells in Culture Part B. Quantitative Fluorescence Microscopy-Imaging and Spectroscopy.* San Diego, CA, Academic Press.
- Teh, SJ, and D.E. Hinton. 1993. Detection of enzyme histochemical markers of hepatic preneoplasia and neoplasia in medaka (*Oryzias latipes*). *Aquat Toxicol* **24**(3–4): 163–181.
- Wakamatsu, Y, Pristiyazhnyuk, S, Kinoshita, M, Tanaka, M and Ozato, K. 2001. The see-through medaka: a fish model that is transparent throughout life. *Proc Natl Acad Sci U S A* **98**(18): 10046–50.
- Webb, W, Wells, S, Sandison, D and Strickler, J 1990. *Criteria for Quantitative Dynamical Confocal Fluorescence Imaging.* New York, Wiley-Liss, Inc.
- Willett, K, Steinberg, M, Thomsen, J, Narasimhan, TR, Safe, S, McDonald, S, *et al.* 1995. Exposure of killifish to benzo[a]pyrene: comparative metabolism, DNA adduct formation and aryl hydrocarbon (Ah) receptor agonist activities. *Comparative Biochemistry and Physiology Part B: Biochemistry and Molecular Biology* **112**(1): 93.

Received 27 March 2007.